Characterization of 12 kDa PVP-OD nanocarriers and the influence of their size on the uptake in mammalian cells

Master Thesis

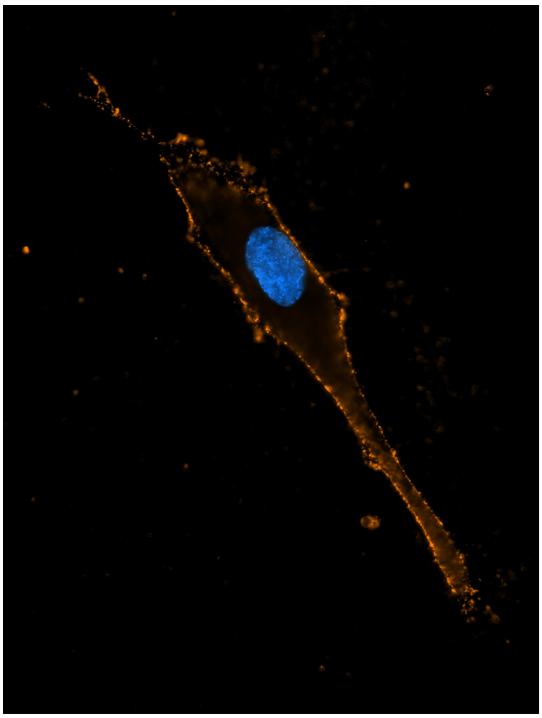

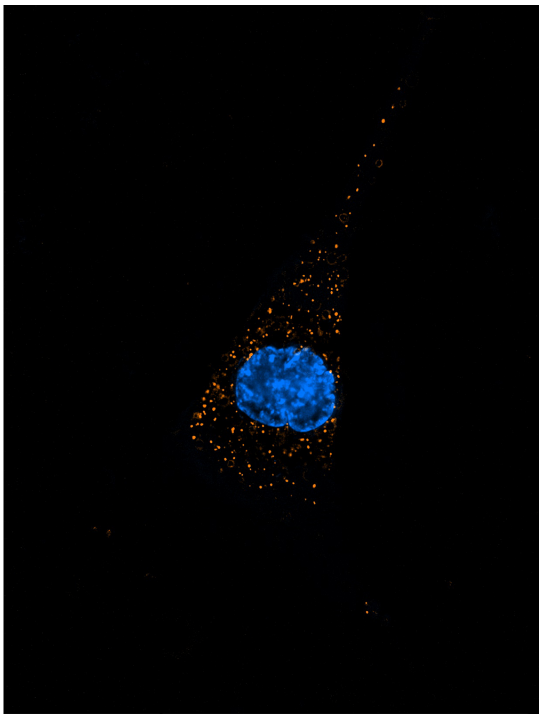

Levi Nelemans

June 10, 2019

AALBORG UNIVERSITY
STUDENT REPORT

Master studies of Nanobiotechnology at department of Materials and Production Faculty of Engineering and Science

Physics and Nanotechnology
Skjernvej 4a
9220 Aalborg Ø

Title:
Characterization of 12 kDa PVP-OD nanocarriers and the influence of their size on the uptake in mammalian cells

Project period:

September 2018 - June 2019

Participants:

Levi Nelemans

Supervisors:

Leonid Gurevich

Total pages: 71
Appendices: 11
Finalized 10-06-2019

Abstract:

Nanocarrier drug delivery systems can greatly improve bioavailability, circulation times and delivery of drugs. Cellular uptake mechanisms of nanocarriers are greatly influenced by their physicochemical properties. In this master thesis, the characteristics of the 12 kDa amphiphilic block copolymer PVP-OD is investigated and the influence of nanocarrier size on the uptake in fibroblasts (CRL 2429) examined. Therefore, nanocarriers with a size of 220 nm (0.2 PDI) and 21 nm (0.244 PDI) were created by sonification or cosolvent evaporation, respectively. Both nanocarriers were taken up by a energy-dependent process, since inhibition led to a decrease of median fluorescent intensity (MFI) of 90 or 97 percent for sonificated and cosolvent evaporated nanocarriers, respectively. Colocalization of the cosolvent evaporated nanocarriers drug with LysoTracker indicated a possible macropinocytosis or clathrin-mediated endocytic uptake. However, further study with different endocytic inhibitors is necessary.

Contents

1 Introduction

Cancer is one of the leading causes of death globally and has a major impact on the health and living quality of humans. Chemotherapy is currently one of the main approaches to combat cancer. However, low bioavailability due to poor solubility, high side effects and drug resistance limit the effectiveness of these chemotherapeutic agents. Due to the lack of selective delivery, the applied dose has to be limited to prevent overall toxicity. Therefore, new drug delivery systems are necessary to improve the efficiency of these agents. [1]

Nanocarriers, such as liposomes, micelles and nanoparticles, have a great potential as drug delivery systems. By encapsulating the drug and shielding it from the environment, the half-life can be greatly improved. Encapsulation will cause longer circulation times, slow down degradation and improve solubility. Even without active targeting the nanocarriers accumulate around tumours (EPR effect), due to their size. Nanomedicine is a rapidly evolving field, from 2013 to 2016 the clinical trials with nanocarriers has tripled [2].

Polymeric micelles with a hydrophobic core and hydrophilic corona are made from amphiphilic block copolymers that self-assemble in aqueous solution. The core can be loaded with hydrophobic drugs that would normally have poor solubility in vivo. A number of polymeric micelles are in late-stage clinical trails as of 2016 [2]. Some of the factors that influence the efficiency and uptake of these polymeric micelles are particle size, shape and surface chemistry.

The main aim of this master thesis is to study the characteristics and the influence of size on uptake of drug-loaded nanocarriers by mammalian cells. The nanocarrier that will be studied is a 12 kDa amphiphilic block copolymer called poly-N-vinyl-2-pyrrolidone thiooctadecyl (PVP-OD, figure 1.1) [3, 4]. The hydrophilic block, PVP is a FDA approved polymer and previous studies have shown the biocompatibility of amphiphilic PVPs and nano-scaled PVP drug carriers [5–7]. Thiooctadecyl is used as an end-group and functions as the hydrophobic block.

This specific nanocarrier has been reported to have different uptake mechanisms depending on size [3]. Sub 100 nm nanocarriers were found to enter the nucleus, while larger nanocarriers were not. Therefore, different sized nanocarriers will be produced and analyzed. Furthermore, the uptake mechanisms of these carriers in mammalian cells will be investigated with the help of endocytosis inhibitors.

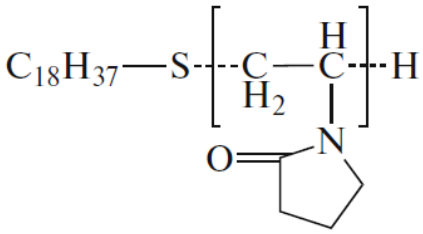

Figure 1.1: PVP-OD block copolymer.

1.1 Polymeric drug delivery systems

Drug delivery systems (DDS) can increase the solubility of hydrophobic drugs, extent circulation times and protect drugs from excretion or breakdown. Specifically the use of polymeric drug delivery systems have been on the rise [2]. This is partly caused by improved polymerization techniques that lead to well-defined structures, narrow molecular weight distributions and tunable properties [8].

In general, a drug delivery system should at least have the following properties [8, 9]:

- The system should be stable during production, storage and use.
- The system should be inert, non-toxic and avoid non-specific interactions inside the body.
- The system should be able to transport the drug to the required target.
- At the target, the system should be able to release the drug in a controlled way.
- The system should be biodegradable and readily eliminated from the body once the drug has been released.

There are a lot of different polymeric drug delivery systems available, such as simple polymer drug conjugates, polymer nanoparticles, polymer-modified liposomes and polymeric micelles. This section will specifically focus on polymeric micelles, since the 12 kDa PVP-OD block copolymer has amphiphilic properties.

1.1.1 Polymeric micelles

Polymeric micelles are a class of amphiphilic block copolymers (ABCs) that are composed of hydrophobic and hydrophilic blocks [9]. Di- or tri-block copolymers are most commonly used to form polymeric micelles [10]. When these polymers are dissolved (in aqueous solution) at a concentration above their critical micelle concentration (CMC) they will self-assemble into aggregates with a hydrophobic core and hydrophilic corona (figure 1.2). Below the CMC, all of the polymers exist as monomers in solution. The CMC values of polymeric micelles are relatively low, creating stable micelles at working concentrations inside the blood [8, 10]. In general, spherical micelles are formed if the copolymer contains longer hydrophilic segments, while nonspherical rods or lamellae are formed with longer hydrophobic segments [8]. The core of these micelles can be used for drug entrapment and

the hydrophobic block will influence the stability and drug release characteristics of the micelle. The corona influences the pharmacokinetic properties in vivo and can be further modified (e.g. active targeting) [11]. PEO or PEG are most commonly used as hydrophilic blocks, while the hydrophobic block varies widely [10, 11].

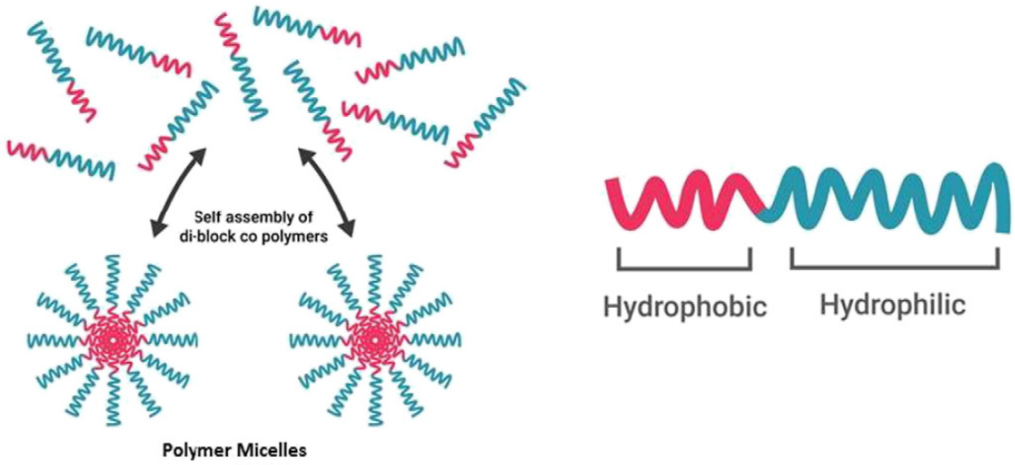

Figure 1.2: Schematic depiction of the formation of micelles above CMC from amphiphilic di-block copolymers. Adapted from [12].

Targeting

Ideally, drug-loaded polymeric micelles travel from the bloodstream to their specific target, without entering other tissues. Due to their small size and extended circulation time, the micelles can accumulate in compromised tissue via an effect known as enhanced permeability and retention (EPR). In normal blood vessels, cells are tightly packed, allowing only small molecules to diffuse through. However, in tumours the vascular structure is compromised, creating 'leaky' blood vessels through which polymeric micelles can diffuse (figure 1.3a). Furthermore, the lymphatic drainage is also decreased, slowing down micelle removal [13]. This phenomenon is called passive targeting, and can occur to nanocarriers as large as 200 nm [11]. The corona of the polymer can be further modified for active targeting with specific ligands, antibodies or peptides, to increase accumulation at the target (figure 1.3b).

1.1.2 Drug loading of polymeric micelles

Drugs can be loaded inside micelles by either a passive approach, based on hydrophobic interactions, or by being covalently linked to the amphiphilic block copolymer (ABC). Obtaining a high drug load using this passive approach remains challenging [14]. This section will give a small overview of some of the current techniques for passive drug loading of polymeric micelles.

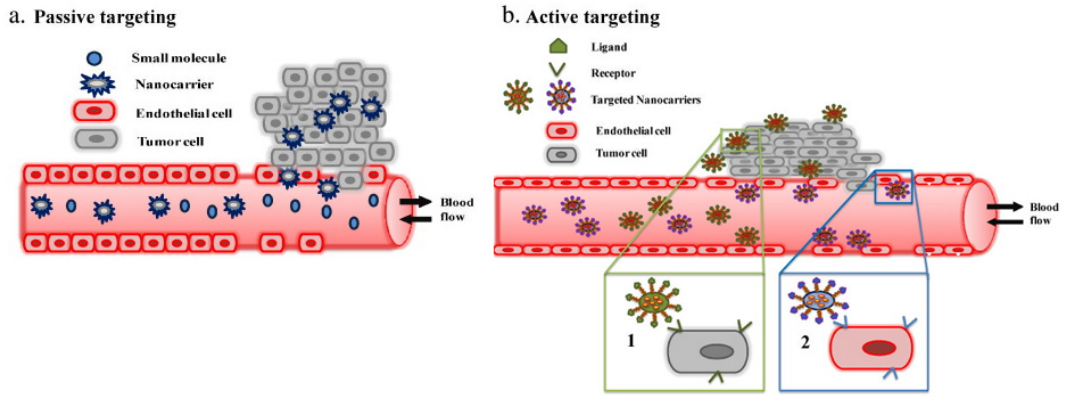

Figure 1.3: a) Passive targeting of polymeric micelles to tumours, due to the EPR effect. b) Active targeting of polymeric micelles to either specific receptors on tumor or endothelial cells. Adapted from [13].

Direct dissolution

This is the simplest technique to prepare drug-loaded micelles and only works for hydrophobic drugs that are somewhat soluble in water. Both the drug and ABCs are dissolved in water and as long as the concentration of the ABC is above CMC, drug-loaded micelles should form. [15]

Solvent evaporation/thin-film formation

In this case, both the drug and ABCs are dissolved in a volatile organic solvent that is completely removed via rotary evaporation. The left over thin-film is then rehydrated in water. [15]

O/W emulsion

This technique makes use of solvents that are non-miscible in water. First, the ABCs are dissolved in water and an organic solvent containing the drug is injected in the water phase, under heavy stirring (figure 1.4a). The drug can then get captured inside the micelles at the interface. [16]

Direct dialysis

The drug and ABCs are dissolved in an organic solvent and put inside a dialysis bag, the organic solvent is dialyzed out and should slowly force the drug inside the micelles (figure 1.4b). [16]

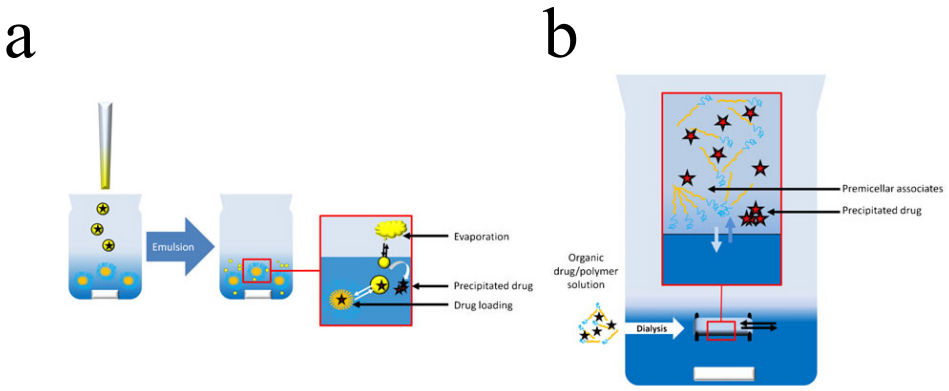

Figure 1.4: Drug loading of polymeric micelles using the (a) O/W emulsion or (b) direct dialysis method. See text for details. Adapted from [16].

Cosolvent evaporation

In cosolvent evaporation the drug and ABCs are first dissolved in a water miscible solvent. Then, water is slowly added to a ratio in which both the drug and polymer can still be dissolved. The mixture is then evaporated until the organic solvent is completely removed. The slow removal of the organic solvent forces the drug to go inside the micellular core as the water concentration increases (figure 1.5). [16]

For both direct dialysis and cosolvent evaporation a good organic solvent is necessary and can drastically change the drug loading capacity . The capacity is lowered if the drug aggregates out of solution before the ABCs have a chance to form proper micelles. Overall, cosolvent evaporation seems to be superior to direct dialysis, since the increase in water concentration can be more precisely controlled. [16]

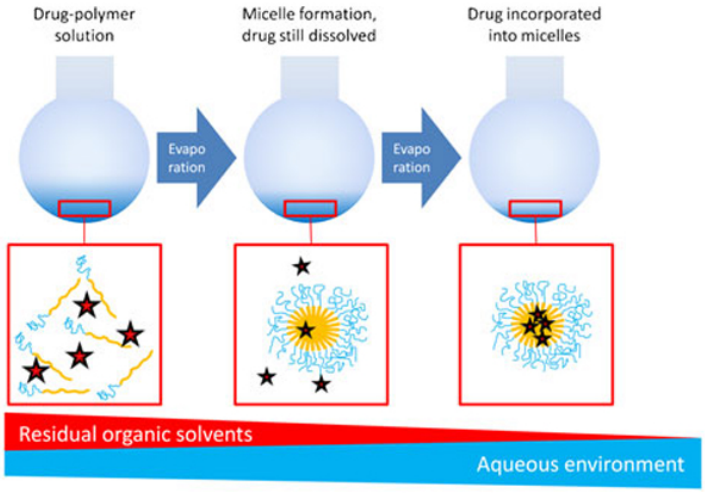

Figure 1.5: Drug loading of polymeric micelles using cosolvent evaporation. See text for details. Taken from [16].

1.2 Endocytosis

Endocytosis is a cellular process in which molecules or macromolecules are internalized. Examples of endocytic processes are the uptake of nutrients, surface receptor regulation and mitosis. The same endocytic pathways are often exploited by pathogens to mediate uptake into cells [17, 18]. The general mechanism of endocytosis consists of four basic steps: 1) Binding interaction at the surface of the cell; 2) cell membrane encapsulation and pinching off; 3) tethering of the vesicle and finally; 4) trafficking of the vesicle within the cell [17].

Even though the different type of uptake mechanisms have been studied for a while, they are still not fully understood. This is caused by the complexity of the processes, overlap of proteins between different mechanisms and the lack of mechanism specific inhibitors. However, with the rise of nanocarriers and specialized drug delivery systems a better understanding of the uptake of these carriers and trafficking within the cell could greatly improve the efficiency of the drug.

Traditionally, endocytosis is divided into two main categories based on the size of the cargo, namely phagocytosis (the uptake of large particles) and pinocytosis (the uptake of fluids and solutes) (figure 1.6). The latter can be divided in multiple subcategories with different uptake mechanisms [17, 19].

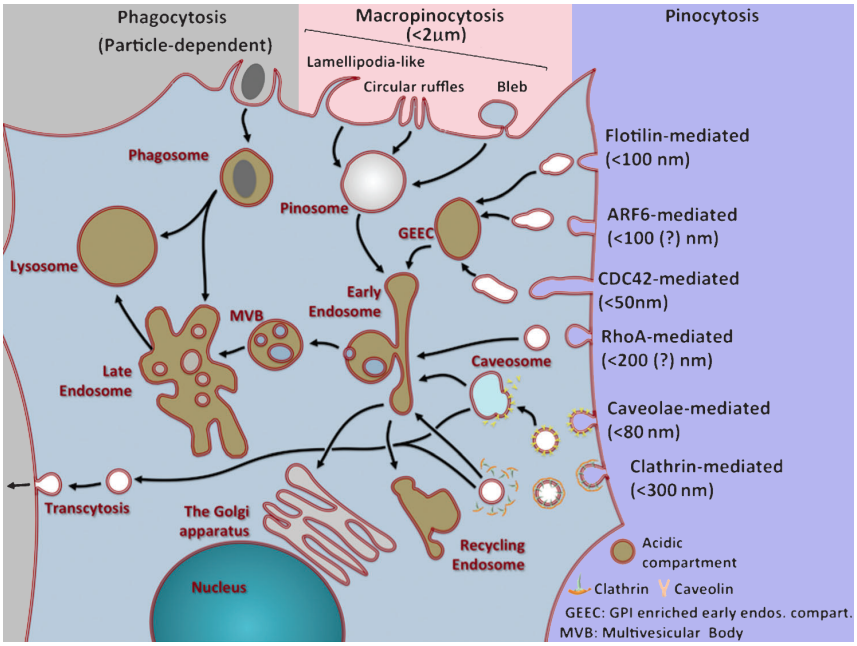

Figure 1.6: Overview of common types of endocytosis with an approximate maximum cargo size for each pathway. Adapted from [17].

1.2.1 Phagocytosis

Phagocytosis is a process that is only performed by a few specialised cells named phagocytes, such as macrophages, neutrophils and dendritic cells. Some other cell types (fibroblasts, epithelial and endothelial cells) might also display phagocytic behavior, but to a much lesser extent [20]. The main task of phagocytes is to kill or remove pathogens, dead cells and cell debris. Before this is possible, the phagocytes should be able to detect the foreign objects. In a process called opsonization, foreign objects are tagged with so called opsonins (IgG, IgM and other proteins). Once tagged, the objects interact with membrane receptors on the phagocyte that induce a cascade of signals leading to ingestion. Actin is assembled around the object, forming membrane protrusions around the particle which will ultimately lead to engulfment, creating a phagosome (figure 1.7). [19, 20]

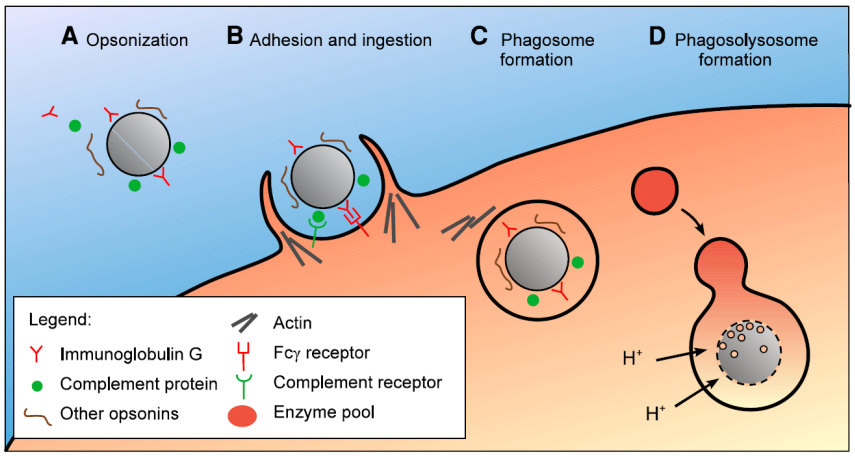

Figure 1.7: Overview of phagocytosis in which an opsonized target gets recognized and phagocytosed, before being broken down. Taken from [20].

Phagocytes have the ability to ingest particles with a diameter up to tens of micrometers. The size limit seems to only be determined by the phagocyte's cell volume. However, Champion et al. showed that the local particle shape has a large influence on induction of phagocytosis (figure 1.8) [21]. Polystyrene particles of different sizes and shapes were used to induce phagocytosis [22]. All particles could induce uptake in at least one direction, but the curvature of the particle at the initial point of contact determined the ability of the phagocyte to engulf the particle. It is suggested that the local particle shape determines the complexity of the actin structures that need to be rearranged to induce phagocytosis. Failure to create these complex structures prevents internalization.

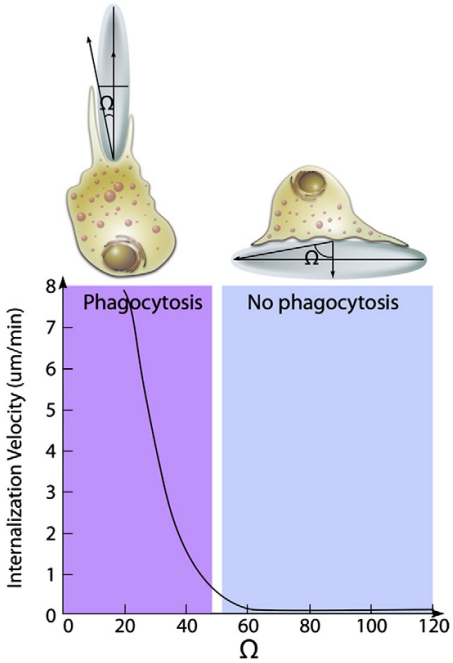

Figure 1.8: The local particle shape influences the uptake of non-spherical particles. Depending on the local contact angle the uptake can be greatly reduced or even halted. Taken from [19].

1.2.2 Pinocytosis

In contrast to phagocytosis, pinocytosis can be found in all cells. There are multiple entry pathways that have distinct differences in cargo, cargo size and uptake mechanism (figure 1.9), these pathways will be further discussed below. [23]

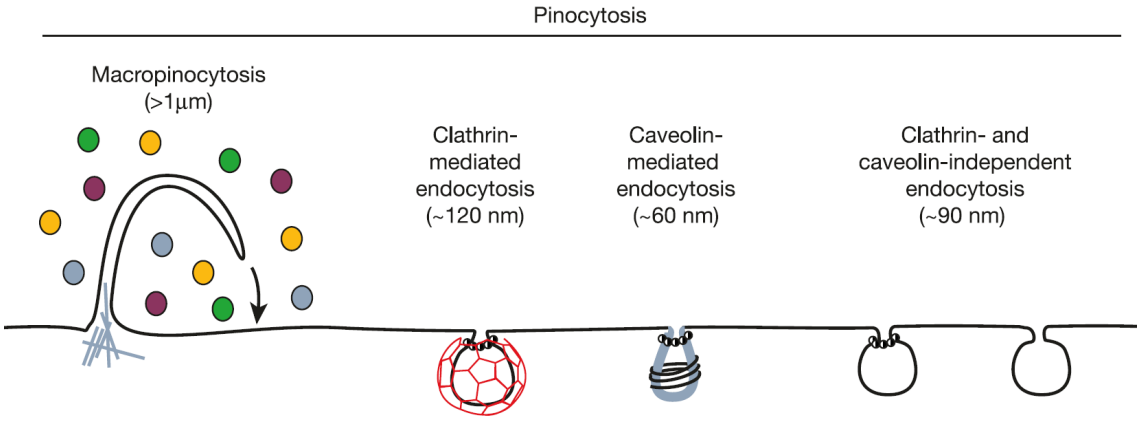

Figure 1.9: Overview of different pinocytosis mechanisms that have distinct differences in cargo, cargo size and mechanisms. Taken from [23].

Clathrin-mediated endocytosis

Clatrin-mediated endocytosis (CME) is responsible for uptake of essential nutrients, down regulation of cell signaling and maintaining cellular homeostasis [19]. It was first discovered

in 1964 by Roth and Porter who observed coated pits and is the most studied endocytosis mechanism to date [17, 24].

CME involves engulfment and upconcentration of transmembrane receptors that are bound to ligands on the plasma membrane (figure 1.10). Coated pits are formed around the cargo on the cytosolic side of the membrane by cytosolic proteins, with as main unit clathrin. Clatrin has a three-legged structure that can self-assemble into closed polygonal cages with the help of adaptor proteins [17, 23]. These so called clathrin-coated pits (CCP) are then pinched off the membrane by a GTPase known as dynamin to form clatherin-coated vesciles (CCV). Once the CCV is detached from the membrane, the clathrin coat will disassemble and the vesicle will undergo further intracellular trafficking [17]. The size of the CCVs seems to be linked to the size of the cargo and sizes up to 200 nm have so far been observed [25].

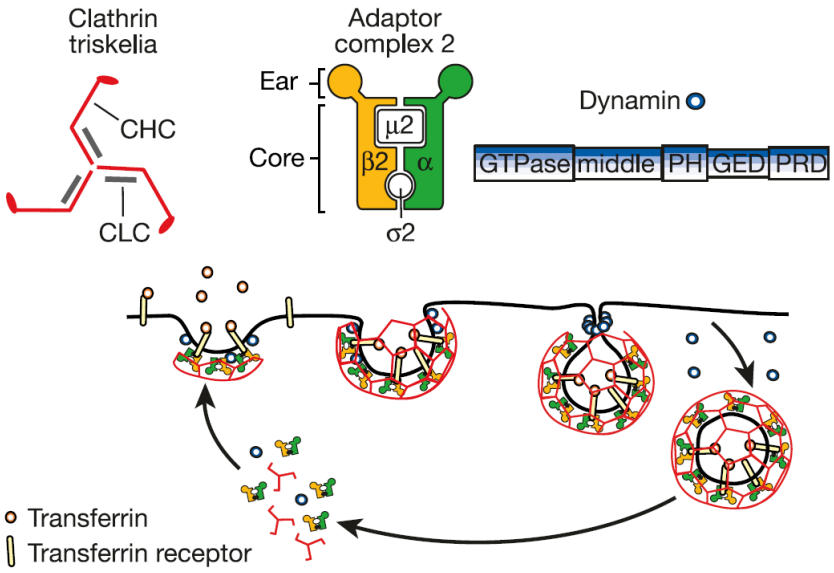

Figure 1.10: Assembly of clathrin with the help of adaptor proteins to form clathrin coated pits (CCP) that, under the influence of dynamin (GTPase), form clathrin coated vesicles (CVV) that get pinched of the membrane. The CCV will disassemble, leaving a "naked" vesicle for further trafficking. Taken from [23].

Caveolae-mediated endocytosis

This pathway plays a role in many biological functions, such as cell signalling, lipid regulation and vesicular transport [17]. Caveolae-mediated endocytosis (CvME) seems to be absent in neurons and leukocytes. This specific uptake mechanism of cargo is not completely understood, but 50-80 nm flask-shaped invaginations can be found on the cell membrane. The protein caveolin-1 (and caveolin-3 in muscle cells) is responsible for the specific shape of the vesicles and can be found as a striated coat on the surface of the membrane (figure 1.9) [23]. Caveolin-1 is a dimeric protein that forms a hairpin structure that can be embedded into the membrane and self associate, it can also bind

multiple molecules including lipids, fatty acids and membrane proteins [19]. Caveolae are most prominently found to be active in transcytosis across endothelial barriers. The caveolae are scissioned of the membrane by dynamin and seem to fuse with caveosomes, surpassing lysosomes. Some nanomaterials are reported to enter cells via caveolae, therefore potentially evading lysosomal degradation [18].

Clathrin- and caveolae-independent endocytosis

Cells that are depleted of chlathrin and caveolin still have some form of endocytosis. These mechanisms are poorly understood and are summarised as being clathrin- and caveolae-independent [18, 19]. These endocytic mechanisms are cholesterol dependent and seem to use lipid rafts on the membrane that are used for sorting and capturing of cargo. Noteworthy examples are the interleukin-2 receptor (IL-2) and rapid recovery of membrane proteins in neurons, which seem to be taken up via a clathrin- and caveolae-independent pathway [23]. Most clathrin- and caveolae-independent processes seem to also be dynamin independent, but more research is necessary.

Macropinocytosis

Macropinocytosis is an endocytic process that is not directly driven by cargo and entails engulfment of a large volume (0.5 - 10μm) of the extra cellular milieu, in so called macropinosomes. This process is associated with active membrane ruffling and can be induced by growth factors, bacteria, viruses and necrotic cells [17]. The signalling cascade is driven by the family of Rho GTPases that activate actin-driven formation of these membrane protrusions. Only some of these protrusions lead to macropinosomes, caused by the protrusions falling back onto the membrane and fusing with it (figure 1.9) [23]. Why only some protrusions result in macropnocytosis and how this process is regulated, is not yet known.

1.3 Endocytosis of nanoparticles

It is important to know the specific uptake pathway and intracellular fate of a nanocarrier to create an efficient drug delivery system. If the nanocarrier cannot escape lysosomal degradation or cannot release its drug efficiently the pharmacological activity will be greatly reduced. The uptake and specific trafficking pathways are mostly dependent on the physico-chemical characteristics of the nanocarrier [20].

1.3.1 Internal trafficking

Cargo that enters the cell through the CME pathway is mostly targeted to degradative lysosomes (figure 1.11b). First, the cargo will be transported to early endosomes (EE) (pH $\sim$6), which will mature into late endosomes (pH $\sim$5). These endosomes will then fuse with prelysosomal vesicles to form lysosomes that contain hydrolases [26]. This

could be a preferred pathway for stable drug-loaded nanocarriers that release their drug via biodegradation, but could also lead to drug degradation of more sensitive drugs. To promote CME uptake of nanocarriers, their surface could be modified with known endocytotic ligands (e.g. Mannose-6-phosphate, transferrin, riboflavin) [27].

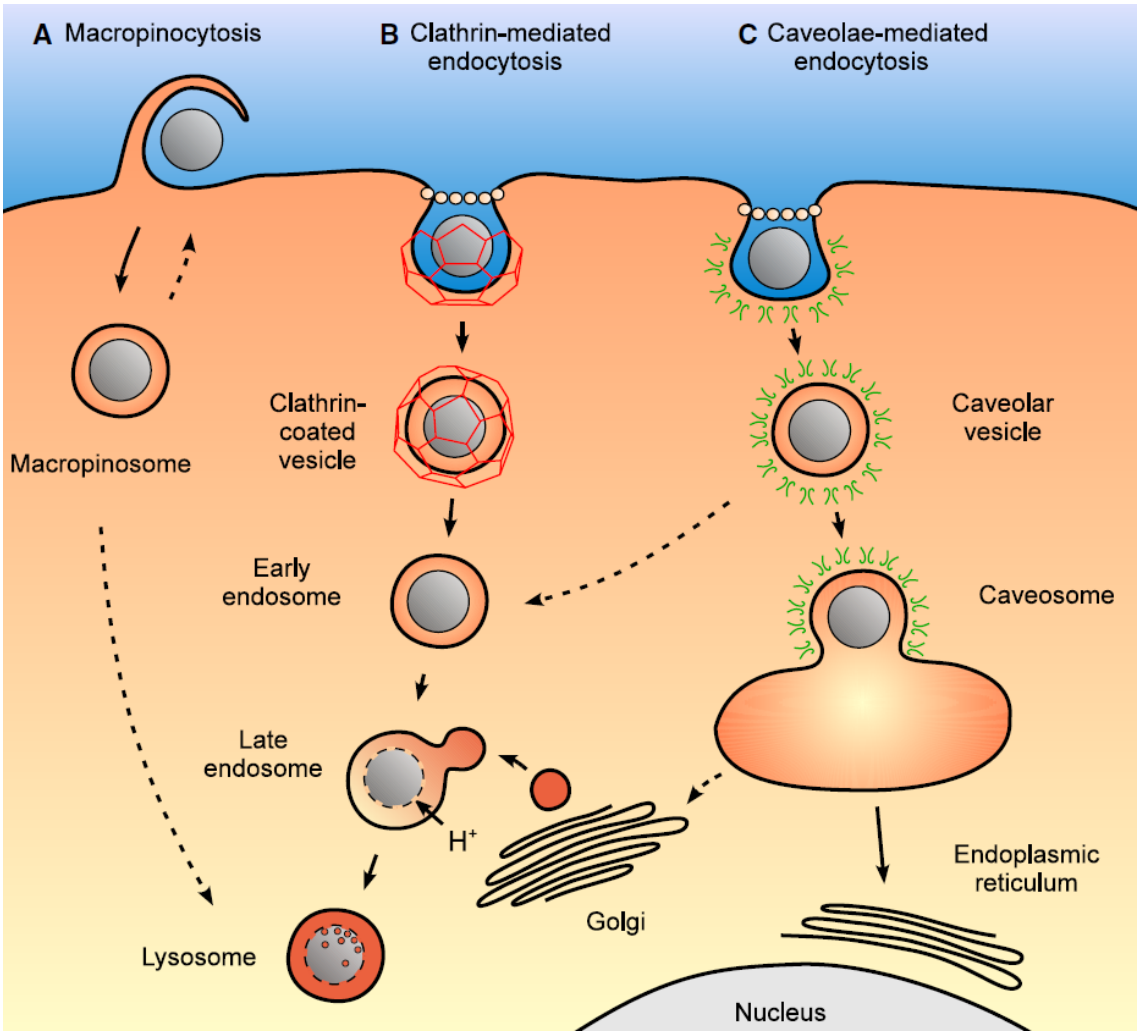

Figure 1.11: Endocytic trafficking of nanocarriers via (a) macropinocytosis, (b) clathrin-mediated endocytosis and (c) caveolae-mediated endocytosis. In which only the caveolae-mediated pathway seems to avoid lysosomal degredation. Taken from [20].

Caveolae are an interesting target for nanocarriers that contain drugs that are highly sensitive to enzymatic break down or pH, since the created caveosomes evade lysosome degradation (figure 1.11c) [20]. Furthermore, caveolae are involved in transcytosis and abundant in endothelial cells, which could be utilized to effectively transport the nanocarriers out of the bloodstream. Examples of ligands that are internalized by CvME include folic acid, albumin, cholesterol and LDL [27].

Macropinocytosis is a quite unselective process and will always occur besides the other pathways, therefore also taking up nanocarriers. The formed macropinosomes might eventually fuse to lysosomal compartments, leading to degradation (figure 1.11a) [20].

1.3.2 Influence of nanocarrier size and charge

The size of the nanocarriers has an influence on the endocytic pathway, but may vary between different cell types and carriers. Optimal particle size for efficient endocytosis was found to be around 50-100 nm, although variation between cells types makes it hard to form any general rules [26]. Interestingly, CME and CvME seem to accept larger sizes of nanocarriers than is typically observed for regular cargo [20]. In general, sizes below 200 nm were found to be involved in CME, while larger sizes shifted to CvME internalization up to a maximum of 500 nm. Nanoparticles below 25 nm were found to internalize via a novel clathrin- and caveolae-independent pathway, which did not show any acidification [28]. This could be a promising pathway for drug carriers that need to avoid lysosomal degradation. However, since the uptake mechanism of nanocarriers varies greatly between carriers and cell types, individual investigation is necessary.
What is commonly observed, is that nanocarriers with a positively charged surface have better association and internalization rates than uncharged or negatively charged carriers [26]. This could be caused by simple electrostatic interactions, since the cell membrane is negatively charged. However, the charge of nanocarriers might also influence the endocytic mechanism. Positively charged PLA-PEG nanoparticles were observed to enter the cell via CME while the same, but negatively charged, nanoparticles were not [29].

1.3.3 Endosome escape strategies

Even when nanocarriers get taken up inside the cell, most carriers end up in endosomes, unable to deliver the drug to the cytosol. Therefore, multiple endosome escape strategies are being developed to deliver the drug inside the cytosol. These strategies usually fall under one of the following categories (figure 1.12) [26]: 1) Breakdown of the nanocarriers inside lysosomes will eventually lead to drug release, this is only applicable when the drug can withstand these harsh conditions; 2) Destroying the endosomes before full maturation; 3) fusion of the nanocarriers with the endosomal membrane to release its contents; 4) active transport of small molecules out of the endosomes.

As an example, the pH in late endosomes and lysosomes is lower than normal physiological conditions. This physiological change is often used as an escape strategy. pH sensitive liposomes based on dioleyl phosphatidyl ethanolamine (DOPE) were developed, which at a low pH, have the ability to fuse with the endosomal membrane and release the drug (figure 1.12) [20]. Also, the polymer poly(ethyleneimine) (PEI) has the ability to disrupt the endosomal membrane and escape degregation. A proton sponge effect was proposed, but recent research cannot confirm this hypothesis [26].

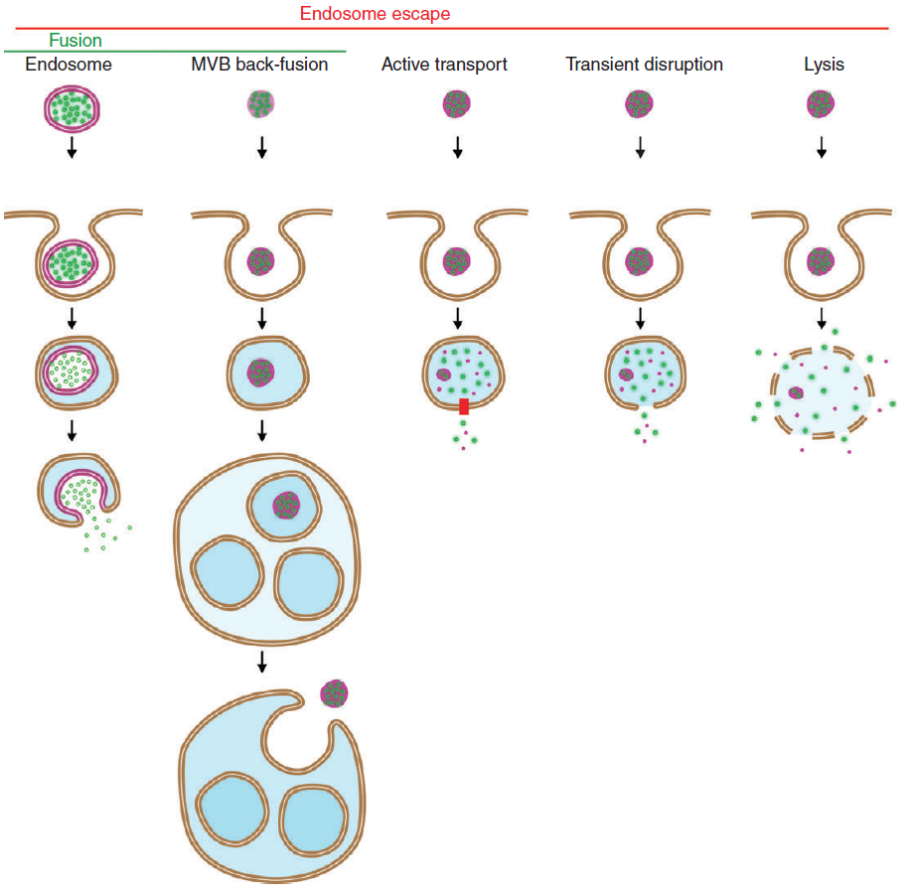

Figure 1.12: Different endosome escape strategies for nanocarriers. Taken from [26].

1.4 Mammalian endocytosis inhibitors

Exposing mammalian cells to nanocarriers will show if and what quantity of carriers will be taken up. However, it does not tell anything about the uptake mechanism(s) that the nanocarriers follow. To further analyse this, specific inhibitors or inhibitory conditions can be used to (partly) block the endocytic pathway. In this master thesis, three different type of inhibitors are used: dynasore, sodium azide and a 4 degree treatment.

Dynasore

Dynasore is a small molecule (figure 1.13) that inhibits the activity of dynamin, a protein responsible for cleaving of the clathrin-coated pits in clathrin-dependent endocytosis and the caveolae in caveolae-mediated endocytosis. Dynasore specifically inhibits the GTPase activity of dynamin, thereby inhibiting the transition from half-formed, U-shaped pits to fully formed pits and from these pits to endocytic vesicles (figure 1.14) [30].

Dynasore inhibition is reversible and inhibition can already be observed after 2 minutes. Unfortunately, dynasore will bind serum proteins causing a reduction in inhibitory activity. Therefore, medium depleted of serum should be used for optimal results. Recently,

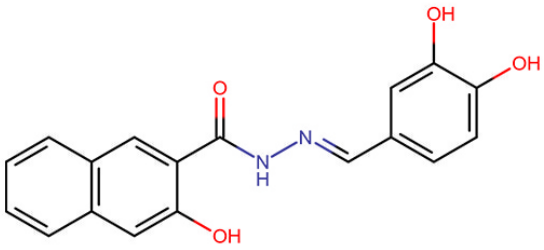

Figure 1.13: Chemical structure of dynasore.

dynasore was found to not only inhibit GTPase activity of dynamin, but to also have wider effects that influence cellular cholesterol, lipid rafts and actin. The exact underlying mechanisms are yet unknown. Therefore, some caution is required when using only dynasore as dynamin blocker, since some off target effects might play a role in cell uptake. [31]

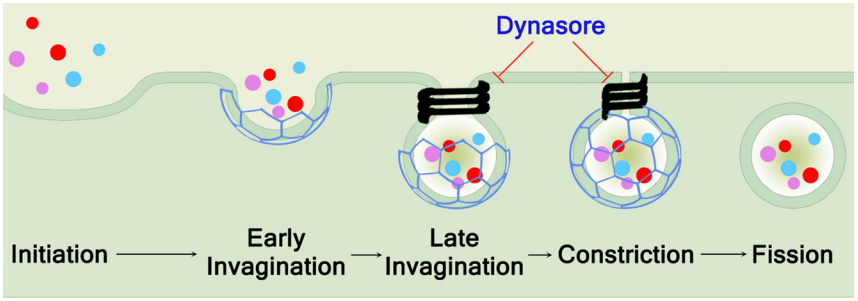

Figure 1.14: Dynasore inhibits clathrin-dependent endocytosis during the late invagination and constriction phase. Taken from [31].

Sodium azide

Sodium azide (NaN_3) has been used in medicine for a long time, for example as additive to prevent bacterial growth [32]. Long-term exposure of sodium azide to mammalian cells will result in cell death. The exact mechanisms of sodium azide are still under investigation, but it is known that it inhibits the respiratory processes inside cells [33]. For example, it has the ability to block cytochrome c oxidase as well as other heme proteins and metalloenzymes [34]. Already small quantities can inhibit the respiratory system, although the cytotoxicity differs greatly between different types of mammalian cells. Above a concentration of 1 μg/mL myocardial, nerve, fibroblast, liver and kidney cells were all suppressed in their respiration [35]. In theory, cells fully depleted of energy should not be able to perform endocytosis. Using sodium azide as an inhibitor could therefore indicate if the uptake process of nanocarriers is energy dependent. This strategy has effectively been used by Chen et al. [36]. It is however necessary to find a concentration that will induce respiratory inhibition, without cell killing.

4 degree treatment

4 °C treatment uses the same principle as the sodium azide treatment. Lowering the temperature of the cells will deplete them of energy, thus inhibiting active endocytosis. This is a common assay to quickly confirm that the nanocarriers follow a classical endocytotic pathway [36–38].

1.5 Autofluorescence

A common problem in fluorescent microscopy is autofluorescene of tissues and cells. The autofluorescence can interfere with the detection of specific fluorescence signals and illuminate different parts than those of interest. This makes distinction between signal and autofluorescence troublesome, especially if the signal of the probes are weak. Autofluorescence is most commonly observed in the FITC range (λ_{max} of 525 nm) [39].

Most often, autofluorescence is not caused by a single source, but by a multitude of factors. In general, we can distinct autofluorescence caused by endogenous tissue, cells and fixation sources. Common sources of autofluorescence in human tissues are reticulin, collagen and elastin [39, 40].
Flavins, reduced NAD(P)H and lipofuscins are the main causes of autofluorescence in cells [41, 42]. Since most of these molecules are related to energy processes within the cell, distinct fluorescent signals can be observed in cell compartments related to metabolism. This can lead to a wrong interpretation of the results. The aromatic amino acids tryptophan, tyrosine and phenylalanine also show autofluorescence, but have a lower excitation and emission wavelength than the FITC range ($\lambda_{excitation}$ = 280, 275 and 260; $\lambda_{emmision}$ = 350, 300 and 280, respectively) [40].
Lastly, formalin and certain serums are known to cause autofluorescence when used in fixation. Induced autofluorescence by formalin is most likely caused by a reaction between formaldehyde with adjacent amine groups known as a Schiff acid-base reaction. The created adducts are intensely fluorescent [41–43].

1.5.1 Ways to reduce autofluorescence

Autofluorescence can be reduced by the use of photobleaching, reducing chemicals and quenching dyes [43, 44]. With photobleaching, fixed tissue or cells are exposed to intense light that quenches the autofluorescence signal prior to treatment with fluorescent probes. However, depending on the experimental setup, this might not always be possible.
Using reducing chemicals, such as sodium borohydrate, can greatly reduce background fluorescence of fixed cells and tissue [45]. Reduction of aldehyde and ketone groups greatly reduces formalin-induced autofluorescence. However, attention is required, since reduction chemicals will also reduce certain fluorphores. Lastly, quenching dyes such as Eriochrome black T or Sudan black B are used to remove autofluoresence by absorbing part of the

fluorescence signals. The downside is that it will remove background fluorescence, but also reduce fluorescent probe signals. Therefore, weak probe signals might become undetectable [44].

1.6 Dynamic Light Scattering

Dynamic light scattering (DLS) will be used to measure the size of the nanocarriers in solution. The following section will give a short overview of the principles behind DLS and is based on the following references: [46–48].

1.6.1 Hydrodynamic diameter

DLS is based on the principle of Brownian motion of particles in solution. The smaller the particle, the faster the Brownian motion will be. The velocity of this motion is described by the translational diffusion coefficient (D) and used to calculate the hydrodynamic diameter $d(H)$ of the particles using the Stokes-Einstein equation:

$$d(H) = \frac{kT}{3\pi\eta D} \tag{1.1}$$

with k, T and η being the Boltzmann's constant, absolute temperature and viscosity, respectively. It is important to have a stable temperature during DLS measurements, since the viscosity of the solvent and thus the Brownian motion are influenced by the temperature of the sample. The calculated size of the particles is referred to as the hydrodynamic diameter and can slightly differ from the actual size, since formula 1.1 assumes the particles to be perfect spheres. However, both the surface structure and shape of the particles can influence the translational diffusion coefficient slightly.

1.6.2 DLS principle

In DLS the Brownian motion is calculated by illuminating the sample and analyzing the intensity change of the scattered light over time. The scattered light will create a certain intensity pattern on the detector, based upon either constructive of destructive interference of the scattered light of the particles. This pattern is rapidly changing due to the movement of the particles over time. In general, smaller particles will cause more rapid intensity fluctuations then larger particles, as seen in figure 1.15 b,c.

This intensity signal is then further processed using a correlator. This device measures the degree of similarity between two signals. In the case of DLS, the similarity of the signal at time = t is correlated to the same signal a very small time interval (nano- or microseconds) later (time = $t + \delta t$). The output gives a result between either perfect correlation (1.00) or no correlation (0.00) and the decrease of correlation over time is influenced by the size

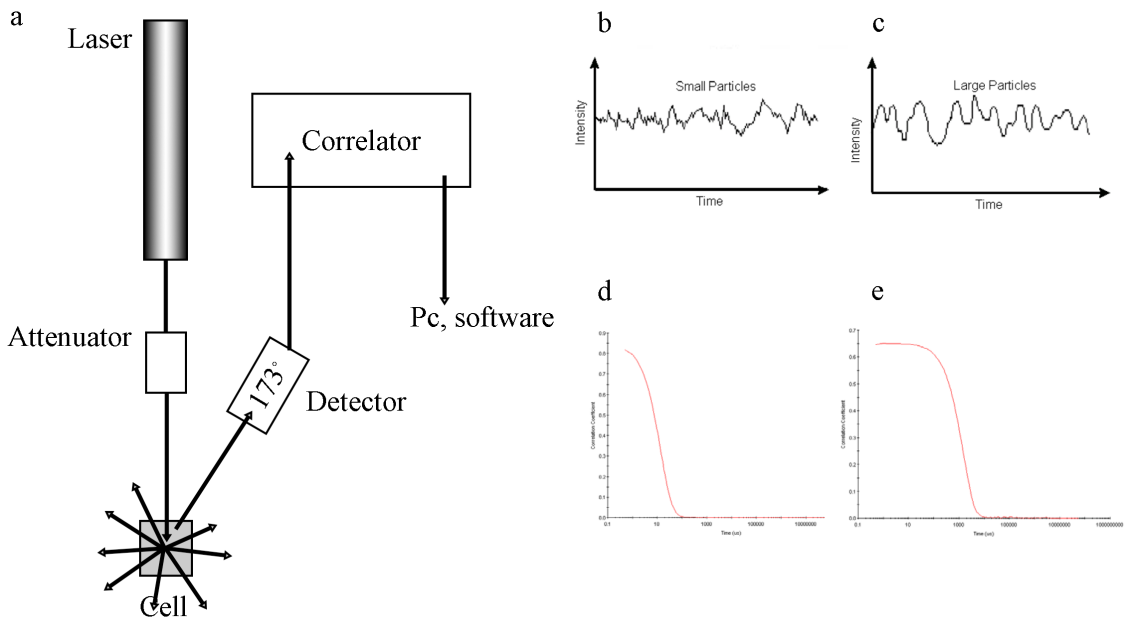

Figure 1.15: a) Overview of the general components in a DLS setup. Fluctuations in the intensity signal are more rapid for (b) smaller particles, (c) compared to larger particles. General correlation function that indicates faster decay for (d) smaller then (e) larger particles. Adapted from: [47].

of the particles. In general, the faster the decay the smaller the particles and the steeper the line the more monodisperse the sample is (figure 1.15 d,e).

Correlation function

The intensity correlation function can be expressed as follows:

$$(\tau) = \langle I(t)I(t+\tau)\rangle \tag{1.2}$$

where, τ is the time delay between two time-points. This function can be normalised:

$$g(\tau) = \frac{\langle I(t)I(t+\tau)\rangle}{\langle I(t)\rangle^2} \tag{1.3}$$

By coupling equation 1.3 to its electric field correlation function (based on the Siegert relation), equation 1.4 can be obtained.

$$g(\tau) = A + B|g_1(\tau)|^2 \tag{1.4}$$

With A being the baseline of the function ($\sim$1) and B the intercept of the correlation function. In case of a monodispersed sample the correlation factor decays exponentially and equation 1.4 can be written as

$$g(\tau) = A + B\exp(-2\Gamma\tau)$$

With Γ being a decay constant $\Gamma = Dq^2$ and $q = (4\pi\eta/\lambda)\sin(\theta/2)$ in which η,λ and θ are the solvent refractive index, wavelength of the laser and angle of the detector, respectively.

If the sample is polydisperse equation 1.4 cannot be rewritten and $g(\tau)$ is the sum of all exponential decays present in the correlation function.

To obtain useful size information various algorithms are used. Fitting a single exponential to the correlation function will give the mean size (z-average diameter) and polydispersity index (PDI) of your sample. Fitting a multiple exponential to the correlation function will give a distribution of particles sizes by their relative intensities. This is known as the intensity size distribution and is most commonlly used.

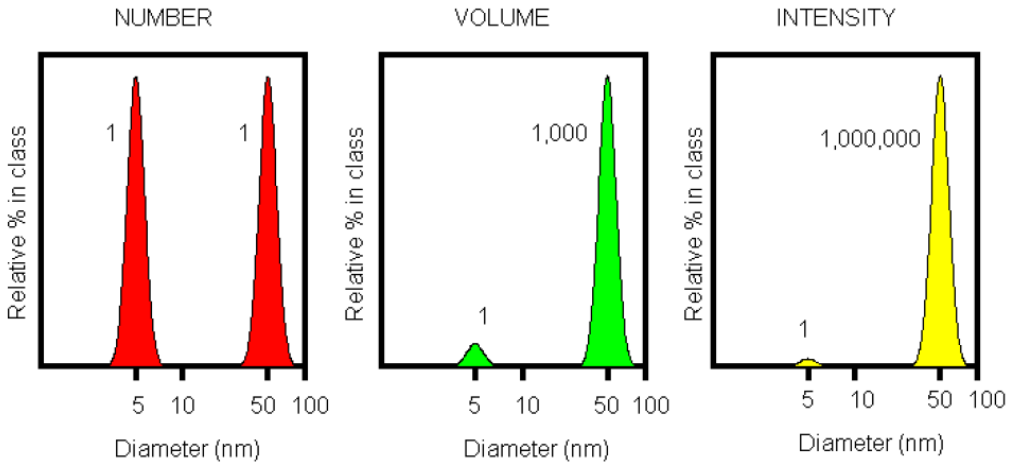

Figure 1.16: The intensity distribution is bias to larger particles ($I \sim R^6$), but can be converted to a volume or number distribution for a better representation. Taken from: [47].

A downside of using an intensity distribution is that the intensity of the scattered light is proportional to r^6. Therefore, large particles or dust can quickly overshadow smaller particles in your sample. Volume or number distributions can be obtained for a more accurate representation of the amount of particles in solution. However, these calculations are still based on the intensity correlation signal and could give inaccurate results.

1.7 Flow Cytometry

Flow cytometry will be used to obtain some statistical data regarding nanocarrier uptake. The following section will give a short overview of some principles behind flow cytometry and are based on the following references: [49, 50].

1.7.1 Light scattering

In its essence, flow cytometry is based on detecting light scattering and (fluorescent) emission of single cells that move past an excitation source (normally a laser beam) (figure

1.17a). The first instruments could only detect the size of the cells, while today up to 14 parameters can be simultaneously detected. Other then detecting cells, some flow cytometry instruments also have the ability to sort the cells. This overview will only focus on the optical system and the information that is gathered, rather then fluidics or specific detectors.

When cells pass the laser, some light will be scattered. This scattered light is detected at two positions, named forward scatter (FSC) and side scatter (SSC) (at a 90°angle). The scattering of the light is influenced by a lot of factors such as the membrane, nucleus, granularity of the cell, shape and surface topography (figure 1.17b). The FSC gives information about cell-surface area, thus indicating the size of the cells. At a 90 °angle from the laser, the detected light is mostly refracted or reflected light. Therefore, SSC gives information about cell granularity or internal complexity.

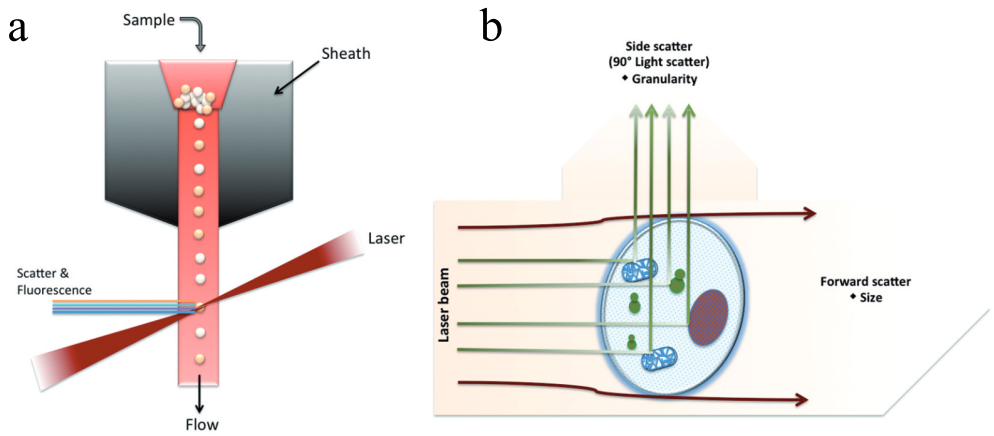

Figure 1.17: a) Working principle of a flow cytometer. b) Effect of light scattering with FSC and SSC being related to size and granularity, respectively. Taken from [50].

The 90 °angle is also used to detect any fluorescent signal. Depending on the type of fluorphores used, a different subset of lasers or filters is needed to capture the signal. Figure 1.18 shows an example of a flow cytometry set up.

1.7.2 Data analysis

Due to the amount of data gathered and the ability to select specific data, flow cytometry is a great tool to analyze complex cell mixtures and filter unwanted particles such as dead cells or debris. This section will be limited to single and two parameter analysis only.

Single parameter analysis

A common plot, mostly represented as a histogram with on the x-axis a specific data value and on the y-axis the number of events (counts). Typically, the data will represent a bell curve with one maximum.

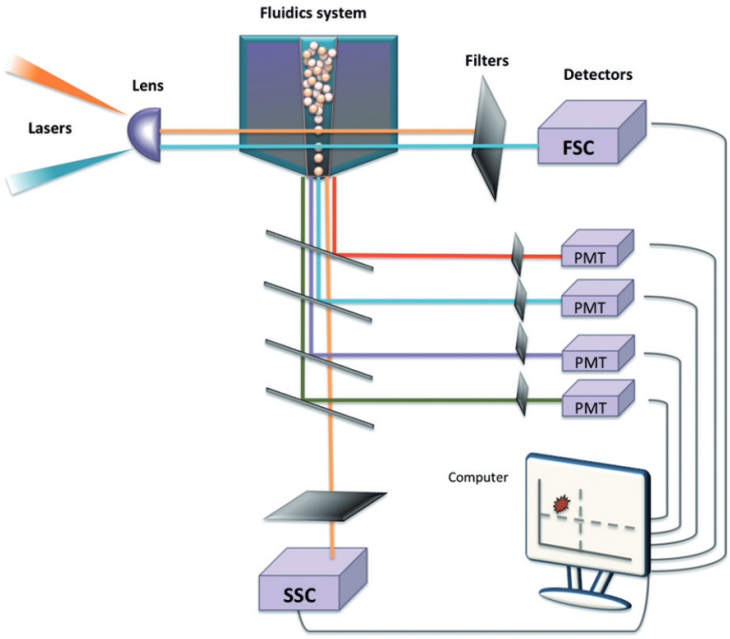

Figure 1.18: Overview of a typical flow cytometry setup. Taken from [50].

Two parameter analysis

Two parameter plots can be displayed in different ways. The most common ones are a dot plot or density plot. The first shows the comparison of two parameters, in which each dot represents an event (figure 1.19a). The density plot also indicates the frequencies of events, giving more information (figure 1.19b).

Gating

'Gating' is a modification process to selectively show cells of interest by creating a subset of data. This selection is mostly performed based on the FSC and SSC data, which will give a two parameter plot showing size vs granularity (figure 1.19). This plot commonly gives enough information to effectively select the wanted cells/data.

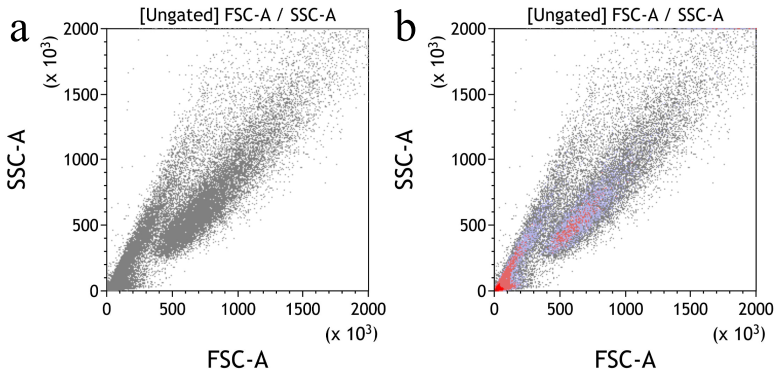

Figure 1.19: Example of a (a) dot plot and (b) density plot of the same FSC and SSC data.

Materials & Methods 2

2.1 Materials

Table 2.1 gives an overview of the specific instruments that were used. Table 2.2 gives an overview of all the chemicals and materials used in this master thesis.

Table 2.1: Overview of all instruments used during this master thesis.

Instrument	Manufacturer	Description
UV-VIS spectrophotometer	Shimadzu	UV-1800
Fluorescence spectrometer	ISS	ChronosDFD
		LX300UV
Rotary evaporator	Ika	RV10 digital
Cooler system	Lauda	Variocool VC600
Sonication probe	Sonics	Vibra cell
Ultrasound bath	VWR	Branson Ultrasonics 2510
Freeze dryer	CHRIST	Alpha 1-4 LD plus
Centrifuge	Eppendorf	5804R
Centrifuge	Hettich	Rotina 280R
Flow cytometer	Beckman Coulter	CytoFLEX S
Fluorescent microscope	Zeiss	Observer z1
		Axiocam mrc5
	Hamamatsu	Digital camera c11440
DLS	Malvern	Zetasizer nano-zs

Table 2.2: Table with overview of chemicals and materials used.

Chemical/material	Manufacturer	Catalog number
Cellulose acetate minisart 0.2 μm filter	Sartorius	16534-k
4-well borosilicate slides	Thermo Fisher Scientific	155383PK
Amicon 15 mL Spin-filter, 30 kDa	Merck	UFC903008
PVP-OD, 12 kDa	Provided from Mendeleev University of Chemical Technology of Russia	[4]
DiI	Invitrogen	D282
Dynasore hydrate	Sigma-Aldrich	D7693-5MG
HOECHST 33342	Sigma-Aldrich	B2261
Europium chloride	STREM chemicals	93-6306
Sodium azide	Merck	8.22335.0100
Lysotracker Green DND-26	Thermo Fisher Scientific	L7526
Water LiChrosolv	Merck	1.15333.1000
Ethanol (96%)	Kemetyl	200-578-6
Acetone	Sigma-Aldrich	34850-1L-M
Tetrahydrafuran (THF)	Sigma-Aldrich	401757-1L
Acetonitrile	VWR	20060.420
Hexadecane	Sigma-Aldrich	46703-100ML
Nitric Acid	Fluka	84392
HCL	Honeywell	30721-1L
DEHP	Sigma-Aldrich	237825
DBP	Acros	406642500
Growth Medium (100%)		
(89%) DMEM/F-12 + GlutaMax or	Gibco	31331-028
(89%) DMEM + GlutaMax	Gibco	61965-026
(10%) Foetal bovine serum (FBS)	Gibco	10270-106
(1%) Penicillin/Streptomycin (P/E) (10 KU/mL)	Invitrogen	15140-122
10% formalin	Acros	119690010
Phosphate-buffered saline (PBS)	Gibco	14200-067
TrypLE	Thermo Fisher Scientific	12604-021
Trypsin/EDTA (T/E)	Invitrogen	15090-046
Trypan Blue	Sigma-Aldrich	93595
DMSO	Sigma-Aldrich	D2650
Sodium borohydrate	Fluka	71320

2.2 Methods

2.2.1 Nanocarrier production

Various sized nanocarriers were created in order to analyze the block copolymer's behaviour and to see the influence of size on the uptake in mammalian cells. This section will list all the methods related to the production of the block copolymer aggregates.

Sonification method, DiI-loaded PVP-OD nanocarriers

100 mg of 12 kDa PVP-OD was dissolved in 10 mL of filtered water, by stirring the solution for 2 hours at 50 °C. Then, 5 mg of DiI was dissolved in acetone and dropwise added to the polymer solution. This mixture was sonificated for 10 min on ice (1 sec on, 2 sec off; amp 40%), before being frozen in liquid nitrogen for approx. 7 min. The frozen sample was then freeze-dried for 2 days. When needed, the lyophilized sample was dissolved to the appropriate concentration and pushed over a 0.2 μm filter to create sonificated, unfiltered aggregates. Some of these aggregates were also spun down over a 30 kDa spin-filter (5000 G for 15 min) to create sonificated, filtered aggregates. This was repeated two times, topping up the sample to 9 mL of water in between. Finally, the size distribution was determined using DLS, before being used in further experiments.

Sonification method, curcumin-loaded PVP-OD nanocarriers

The curcumin-loaded nanocarriers were kindly provided by a group of summer-students. The preparation of the aggregates were similar as described above, except curcumin was used instead of DiI.

Sonification method, Europium-complex-loaded PVP-OD nanocarriers

The preparation of the nanocarriers were similar as described above, except 1 mL of chelated europium in hexadecane was added instead of DiI.

Cosolvent evaporation, DiI-loaded PVP-OD nanocarriers

Either 30 or 100 mg of 12 kDa PVP-OD and 3 mg of DiI were dissolved in 100 ml of 96% ethanol, by slow addition under heavy stirring and continued mixing for 2 hours. Then, 10 mL of filtered chromatography water was drop-wise added to the solution. For the creation of pH adjusted nanocarriers, the filtered water was adjusted to a pH of 10. Finally, the solution was evaporated using a rotary evaporator at 40 °C until approximately 3 mL of solution was left. The final solution was then pushed over a 0.2 μm syringe filter. The obtained nanocarriers were analysed using DLS before being used in further experiments.

2.2.2 Characterisation of 12 kDa PVP-OD

Solubility of PVP-OD and DiI in different solvents

To optimize cosolvent evaporation the best solvent for both PVP-OD and DiI was determined. Therefore, 20 mg of 12 kDa PVP-OD was dissolved in 10 mL of ethanol, THF, ACN or acetone at room temperature for 2 hours and analyzed using DLS. Also, 1 mg of DiI was dissolved in 100 μL of THF, ACN, acetone or ethanol. Then, drops of 10 μL of water were added and mixed, until precipitation of DiI was observed.

Stability of PVP-OD in water/ethanol mixtures

20 mg of 12 kDa PVP-OD was dissolved in 96% ethanol. The water concentration was drop-wise increased using filtered water and analysed using DLS every 5% increase, starting from 5% water, till 95% water. They same experiment was performed using pH 10 adjusted water, but the samples were only analyzed at a water concentration of 50, 75 and 95% . Some samples were send of for TEM analysis.

Chelated Europium-complex

To observe the core structure of the nanocarriers using TEM, a chelated Eu-complex was created that could be loaded into the aggregates instead of DiI. Therefore, 29 mg of $EuCl_3 \cdot H_2O$ was dissolved in 5 mL of filtered water adjusted to pH 1 with either HCL or Nitric Acid. Then, 27 μL DEHP or 16 μL of DBP was added to 25 mL of hexadecane. Both solutions were thoroughly mixed for 1 hour, before letting the layers separate. The organic phase was removed and should contain the chelated complex. The complex was further analysed using spectroscopy.

Transmission Electron Microscopy (TEM)

The samples were deposited on a carbon-coated glow discharged 400 mesh nickel grids, stained with one drop of 0.5% phosphotungstic acid (PTA), and imaged with Jeol JEM-1010 transmission electron microscope operating at 60 kV.

Statistical analysis of TEM images

Some of the obtained TEM images were further analysed to compare the size distribution of DLS with TEM. The area of the particles was calculated using the "analyse particles" plugin within ImageJ (1.52n) and the macro's used can be found in Appendix A.5. The obtained area of the particles was then converted into their diameter, assuming the particles were a perfect sphere. This data was plotted into a histogram using Matlab (R2017b and R2018b).

Dynamic light scattering

The size of the nanocarriers was determined by DLS. Measurements were performed in triplo under automatic detection settings and analyzed by Zetasizer software (7.11). Obtained distributions were further analyzed using Matlab (R2018b).

2.2.3 Standard cell culture methods

The following sections will list a brief explanation of standard cell culture methods. Standardized volumes can be found in table 2.3. In-depth protocols can be found in Appendix A.4. All media have been pre-heated to 37 °C to prevent chocking of the cells.

Table 2.3: Standard used volumes for cell culture in mL. T/E stands for Trypsin/EDTA mixture.

Flask size	Medium	PBS	T/E
T175	30	15	3
T75	15	9	1.5
T25	5	3	1

Start of a cell culture and changing medium

Stock of the specific cell culture was defrosted and added to basic growth medium. The solution was spun down (300 G, 5 min) to remove DMSO and resuspended in fresh medium, before being seeded out. When the growth medium was depleted (approx. 2-3 days), it was removed and changed with fresh growth medium.

Sub culturing cells

When the cells were grown to the required confluence, they were either used for experiments or re-seeded. Therefore, the medium of the cell culture was removed and washed with PBS (3x). The appropriate volume of Trypsin/EDTA (T/E) or TrypLE was added and evenly distributed, before being incubated for 3-5 min at 37 °C. To stop the trypsination process, basic growth medium was added equivalent to 3x the volume of T/E. The cells were spun down (300 G, 5 min) and resuspended in fresh growth medium (5 mL). The cells were either used for an experiment or re-seeded for further cultivation. Therefore, 1/10 of the volume was seeded in a new flask with the appropriate standard growth medium.

Counting cells

Cells have to be counted, in order to seed cells with an appropriate concentration. Therefore, cells were first trypsined, as described above. A hemocytometer was assembled and 10 μL of cell suspension was mixed with 10 μL of trypan blue. 10 μL of this solution was applied in the hemocytometer and the cells were counted. The final concentration was calculated according to standard protocol.

Cryopreserving cells

Cells can be preserved for later cultivation. Therefore, the cells were resuspended to a concentration of $2 \cdot 10^6$ cells/mL. The entire volume was distributed into cryotubes with aliquots of 695 μL. Then, 230 μL FCS and 75 μL DMSO were added to each tube and put at -80 °C for 24 hr, before being moved to -140 °C.

2.2.4 Nanocarrier uptake in mamallian cells

The following section will give an overview of different methods that were used to analyse the uptake of the nanocarriers in mammallian cells. All of the cells described below

(fibroblast (CRL 2429) and/or glioblastoma (U87) cells) were first seeded to a density of ca. 5000 cells/cm^2 in a 4 or 8-well borosilicate chambered slide and incubated for 24 hr at 37 °C, before any experiments.

Influence of HOECHST stain and autofluorescence of fixated cells

To verify that the measured signal was coming from our probe, the influence of the HOECHST dye and autofluorescence of the cells in the FITC channel were measured. Growth medium was removed and the cells were washed with PBS (2x). The cells were incubated with DMEM for 30 min at 37 °C. After this, the wells were incubated with DMEM or 0.5 μg/mL sonificated nanocarriers in DMEM as indicated in table 2.4, for 5 min at 37 °C. The wells were washed with PBS (3x) and incubated with 4% formaldehyde with or without HOECHST stain (1:1000) (see table 2.4) for 15 min at 37 °C. Finally, selected wells were treated with sodium borohydrate for 2x 5 min at 37 °C.

Table 2.4: Table giving the different experimental conditions used to investigate autofluorescence and HOECHST influence using both sonificated filtered an unfiltered nanocarriers.

Wells	Experimental condition
1	nanocarriers + HOECHST
2	HOECHST
3	nanocarriers
4	nanocarriers + BH_4

Time-interval experiment

To see the influence of the PVP-OD nanocarriers on the cells over time, a time interval experiment was performed. fibroblast and glioblastoma cells were prepared, their growth medium was removed and the cells were washed with PBS (2x). Then, 0.5 mg/mL of sonificated, unfiltered nanocarrier solution in DMEM was added to all wells. The cells were incubated for 10, 30, 60, 90 and 120 min at 37 °C. After incubation, the cells were imaged live using a fluorescent microscope.

Optimizing nanocarrier concentration

The nanocarrier concentration was optimized to find an optimal concentration that would reduce cell killing, but was still detectable under the fluorescent microscope. Therefore, the medium was removed and washed with PBS (2x), either 0.2, 0.1, 0.05 or 0.01 mg/mL of cosolvent evaporated nanocarriers in DMEM were added and incubated for 2 hours at 37 °C. The media was then removed and the wells were washed with PBS (2x) and incubated with 1:1000 HOECHST in PBS for 10 min, 37 °C. Finally, the medium was removed and washed with PBS (2x) before being stored in PBS and imaged live.

Optimizing effective sodium azide concentration

The cells were washed with PBS (2x) and preincubated with either 1, 0.1, 0.05 and 0.01% sodium azide in DMEM and incubated for 2.5 hours at 37 °C. Then, the cells were imaged using a inverted microscope and their morphology was examined.

Standard nanocarrier uptake experiment

To investigate the uptake mechanisms of the PVP-OD nanocarriers, cells were exposed to the nanocarriers with or without certain inhibitors. This section will only describe the general protocol, specific concentrations of inhibitors and nanocarriers or deviations from the standard protocol will be indicated in the figures.

Growth medium was removed and the cells were washed with PBS (2x). The wells were then treated as indicated in table 2.5. After the incubation steps, the wells were washed with PBS (3x), before being incubated with PBS or DMEM containing HOECHST stain (1:1000 or 1:500) and in some cases 75 nM LysoTracker Green for 15 min at 37 or 4 °C. Finally, the cells were imaged live using fluorescent microscopy.

Table 2.5: Overview of different uptake conditions. All solutions in step 1 and 2 were made in DMEM and the exact concentration of dynasore and sodium azide will be indicated in the figures. Solutions containing dynasore or sodium azide in step 1 were pre-incubated for 30 min or 1 hour, respectively. Well 4 was kept at 4 °C for the entire incubation period and preincubated with cold DMEM for 1 hour.

Wells	Step 1	Step 2
1	DMEM	Nanocarriers
2	Dynasore	Dyansore + nanocarriers
3	Sodium Azide	Sodium azide + nanocarriers
4	Cooled down to 4 °C	Nanocarriers at 4 °C

Fluorescent microscopy

The cells were imaged using a Zeiss inverted microscope and imaged using a 63x water objective. The specific exposure time for each channel can be found in the figures. The filter-sets for each fluorescent dye can be found in table 2.6. The images were further processed using ZEN (blue edition, 2.5) software.

Table 2.6: Overview of the selected filter-sets for each fluorphore.

Fluorescent Dye	**Filter-set**
HOECHST 33342	49
DiI	43 HE
Curcumin	38 HE
LysoTracker Green DND-26	38 HE

Flow cytometry

Control and 4 °C treated cells that were exposed to either sonificated or cosolvent evaporated nanocarriers, were also analyzed by flow cytometry. The incubation procedure was the same as the "standard nanocarrier uptake experiment" described above, with the exception that the cells were in T25 flasks while being exposed. After the incubation, the cells were trypsinized using TrypLE, spun down (330 G, 5 min) and resuspended in PBS. These cells were analyzed using a flow cytometer with a flow rate of 30 μL/min and a total of 20,000 events. The nanocarriers signal was measured, using the PE filter set. The data was further processed using Matlab (R2018b).

Results 3

The following sections will describe the most relevant results that were obtained during this master thesis. First, the characteristics of PVP-OD nanocarriers are analyzed and different drug loading techniques were used to produced different size distributions. Finally, the effect of size of these nanocarriers on uptake in mammalian cells is further investigated.

3.1 Characteristics of PVP-OD nanocarriers

3.1.1 Sonificated nanocarriers

Initially, loaded nanocarriers were produced using the previously described sonification method [3]. This yielded nanocarriers with a diameter of 220 nm (0.2 PDI) according to DLS (figure 3.1a). Regardless of slight modifications to the protocol, the previously described broad distribution (20 - 200 nm) could not be reproduced (Appendix, figure A.7b). Filtering these nanocarriers over a 30kDa spin-filter to remove potential sub-100 nm particles, did not seem to alter the size distribution (figure 3.1a). It should be noted that DLS will produce a intensity distribution which is highly biased towards larger particles and that the original distribution was obtained using NTA. Appendix, figure A.7a shows the numbered distribution obtained for the same data as figure 3.1a, but is also not comparable to the original distribution (Appendix, figure A.7b).

The filtered and unfiltered nanocarriers were also analyzed with TEM, to verify the DLS measurements, investigate their shape and calculate their distribution (figure 3.2). A broad size distribution of nanocarriers was observed and the filtered nanocarriers appeared to be more round in shape then the unfiltered carriers (Appendix, figure A.11). The TEM data was converted into a size histogram (figure 3.1b) which shows a broad size distribution, with a maximum count of 50-75 nm or 100-125 nm for unfiltered and filtered nanocarriers, respectively. The filtered nanocarrier distribution indicates that the 30 kDa spin-filter did not successfully remove the nanocarriers below 100 nm, like previously shown [3]. In conclusion, new drug-loaded, sonificated nanocarriers were created with a different distribution then previously reported.

To visualize the core of these aggregates under TEM, a chelated europium complex was created that could be loaded inside the sonificated nanocarriers. This complex shifted the excitation and emission of europium (Appendix, figure A.15) compared to water,

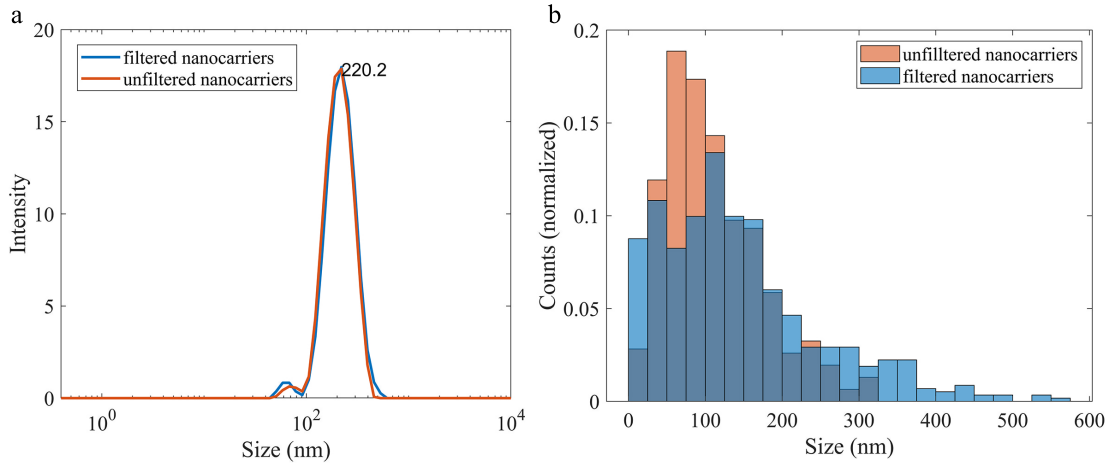

Figure 3.1: a) Average (triplo) intensity distribution of filtered and unfiltered, sonificated nanocarriers. b) Normalized, numbered distribution (bin size=25) of filtered and unfiltered, sonificated nanocarriers obtained from sizes analysis of TEM images with n=568 and n=462, respectively.

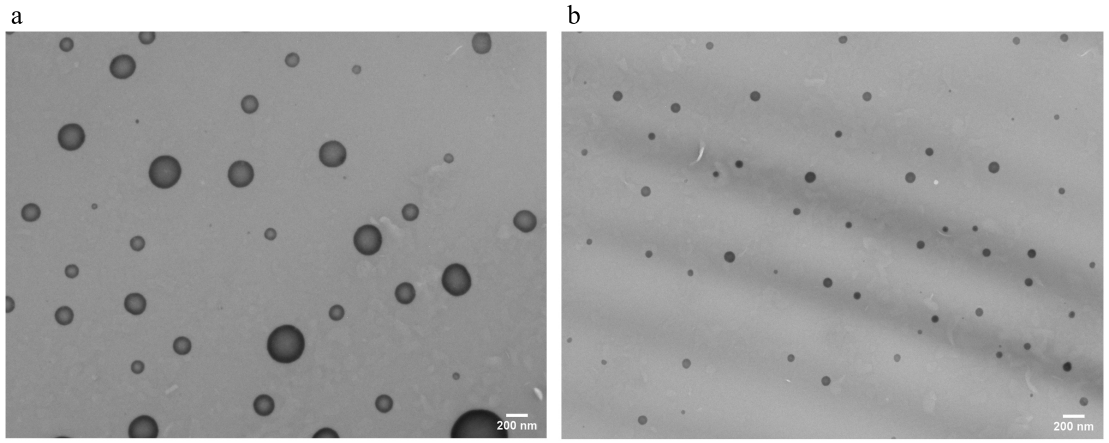

(

Figure 3.2: TEM image of (a) filtered and (b) unfiltered sonificated nanocarriers. Stained with 0.5% PTA.

possibly confirming the correct formation of the complex. While the sonification method did produce nanocarriers of the same size, TEM showed large crystals besides nanocarriers, indicating incorrect loading or possible deconstruction of the complex. No further attempts were made and the composition of the sonificated nanocarrier core remains unknown.

3.1.2 Optimizing solvent for cosolvent evaporation

As described above, dissolving the 12 kDa PVP-OD polymer in water always resulted in an average nanocarrier size around 200 nm. Based on the polymers length, it would be impossible to form actual micelles of this size. Therefore, the dissolved PVP-OD polymer most likely forms some type of larger aggregates in water and a better solvent should be found to properly dissolve the polymer. Furthermore, to obtain high drug loading

with cosolvent evaporation, a water miscible solvent has to be found that dissolves both the drug and polymer. Ethanol, tetrahydrofuran (THF), acetonitrile (ACN) and acetone were used to dissolve the polymer and the obtained size distributions can be found in the appendix, figure A.10. Acetone did not fully dissolve PVP-OD, all the other solvents did. The average size of the polymer in ethanol is around 30 nm, while the size in THF and ACN is around 15 nm. The polydispersity of the polymer was comparable between the solvents. Lastly, drop-wise addition of water caused immediately, visible aggregation of PVP-OD in THF and ACN. Therefore, the optimal solvent for 12 kDa PVP-OD can be described as follows:

$$Ethanol > THF = ACN > Acetone$$

Ethanol was chosen as new solvent, since at least some addition of water to the polymer/drug mixture is required for cosolvent evaporation. It should be noted that DiI did dissolve better in ACN and THF then ethanol.

3.1.3 Stability in water/ethanol mixtures

PVP-OD dissolved in 96% ethanol formed small aggregates around 30 nm. Water (pH 7 or 10) was slowly added to this solution and the size distribution change observed (figure 3.3). When treated with neutral water (figure 3.3a) the nanocarriers remained relatively stable till 75% ethanol, after this larger aggregates were observed. Slow addition of pH 10 water (figure 3.3b) stabilized the nanocarriers up until 50% ethanol. A basic environment seemed to stabilize the PVP-OD nanocarriers up to a higher water concentration.

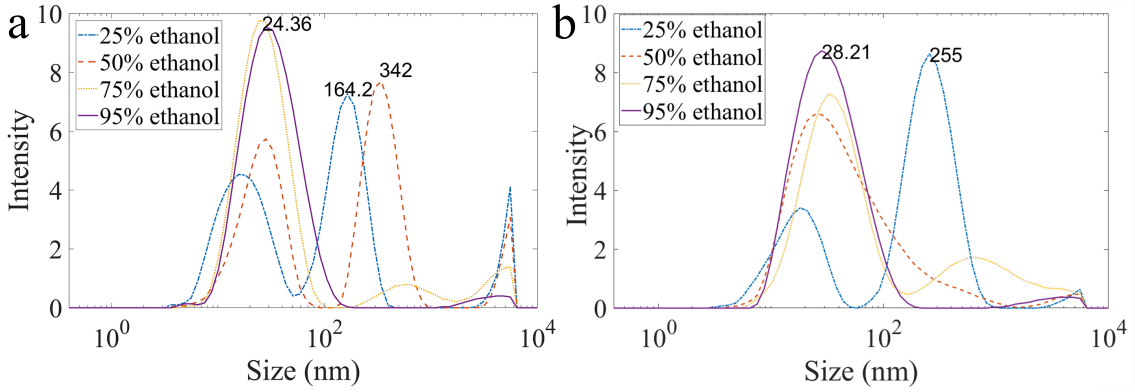

Figure 3.3: Average (triplo) intensity distributions of nanocarriers in different ethanol/water mixtures. Either adjusted with (a) neutral or (b) pH 10 water.

Some of these "empty" nanocarriers in 80% ethanol were further analyzed with TEM (Appendix, figure A.12). While both of the samples were not stable enough to match the DLS distribution (figure 3.4a) and showed larger aggregates (figure3.4b), the sample with pH adjusted water did retain smaller particles. In conclusion, the formed nanocarriers seems to be more stable when the water is adjusted to a pH around 10.

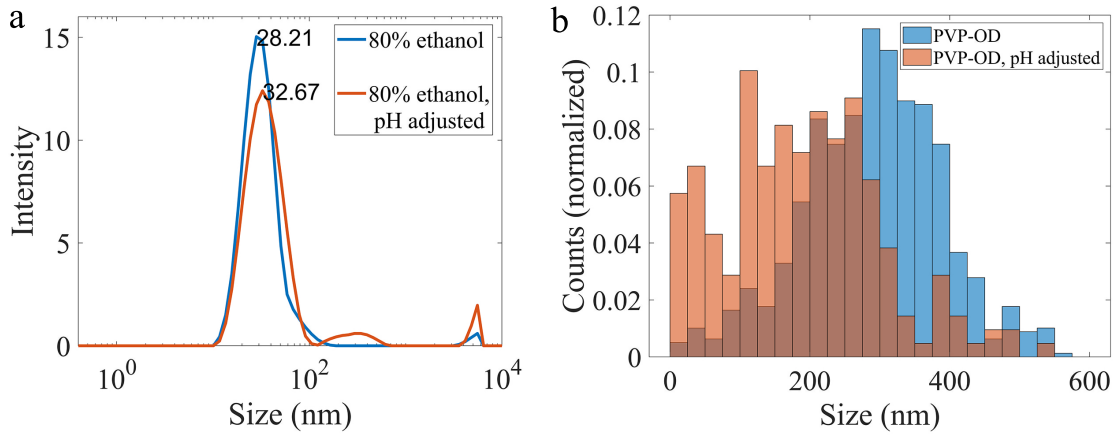

Figure 3.4: a) Average (triplo) intensity distribution of empty nanocarriers in 80% ethanol with neutral or pH 10 water. b) Normalized, numbered size distribution (bin size=25) of nanocarriers made with neutral and pH ajusted (pH 10) water obtained from size analysis of TEM images with n=789 and n=209, respectively.

3.1.4 Cosolvent evaporated, DiI-loaded nanocarriers

New, DiI-loaded nanocarriers were created using the cosolvent evaporation method, with either neutral or pH 10 adjusted water. This yielded nanocarriers with an average size of 38 nm (0.431 PDI) and 21 nm (0.244 PDI), respectively (figure 3.5a). TEM analysis of these samples showed large, irregular shapes for the neutral nanocarriers, while the pH adjusted nanocarriers had a more round appearance (Appendix, figure A.13). A numbered distribution of the pH adjusted nanocarriers was created (figure 3.5b) and has a maximum count between 30-40 nm. This distribution is some what comparable to the DLS distribution of the same nanocarriers, although a size shift towards larger aggregates is observed.

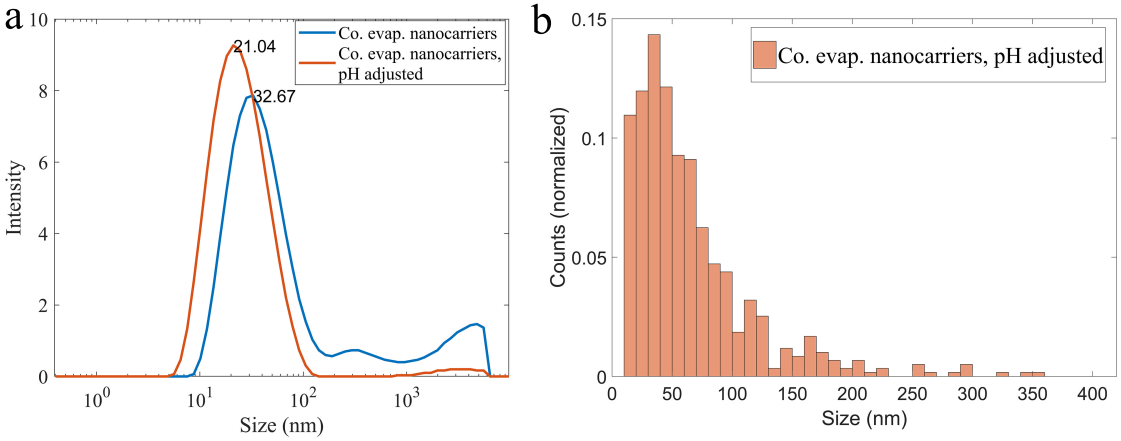

Figure 3.5: a) Average (triplo) intensity distribution of neutral and pH 10 adjusted, cosolvent evaporated nanocarriers. b) Numbered distribution (bin size=10) of pH adjusted, cosolvent evaporated nanocarriers obtained from size analysis of TEM images with n=593.

Stability of DiI-loaded nanocarriers

The stability of these new nanocarriers in solution were investigated, and larger aggregates appear after three weeks (figure 3.6a). Analyzing this three week old sample using TEM, showed a lot of larger aggregates that were not in agreement with the DLS measurement (Appendix, figure A.14). It has proven difficult to image these delicate nanocarriers with TEM, since the nanocarriers tend to aggregate into larger particles during the process. Figure 3.6b shows the stability of the nanocarriers in DMEM medium over a total period of 3 hours. No change in size seems to occur.

Lastly, repeating the same cosolvent evaporating protocol did not always produce nanocarriers of similar size. Sometimes larger aggregates (300-500 nm) would also form, which seemed to be able to pass the 0.2 μm filter (Appendix, figure A.16).

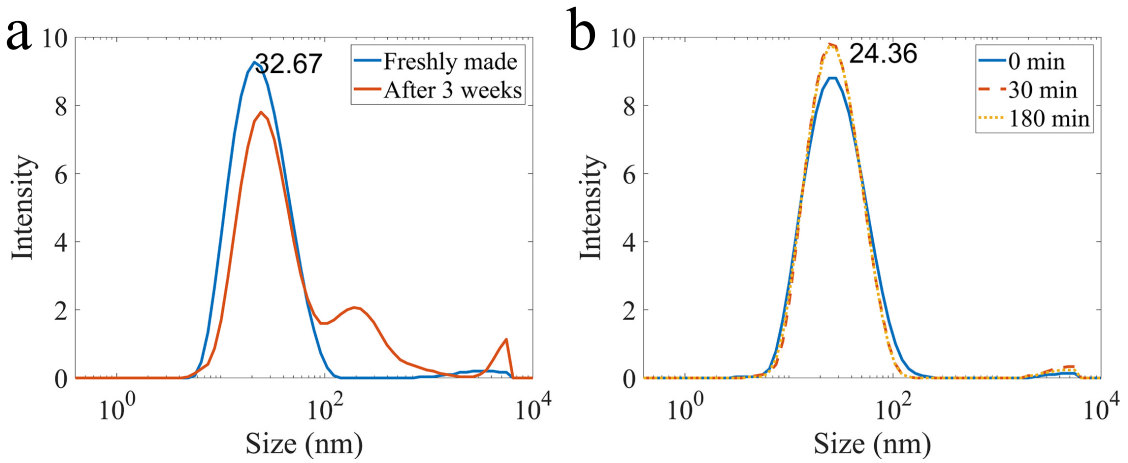

Figure 3.6: Average (triplo) intensity distribution of pH adjusted, cosolvent evaporated, DiI-loaded nanocarriers (a) over time and in (b) DMEM medium.

3.2 Cell uptake experiments

3.2.1 Sonificated, curcumin-loaded nanocarriers

Initially, the sonificated nanocarriers were loaded with curcumin and exposed to fibroblasts and glioblastoma cells. Curcumin is an excellent hydrophobic model drug since it has poor solubility in bulk, appears to have anti-cancer properties and is fluorescent [51–53].

However, the first set of experiments showed that curcumin might not be an ideal fluorescent molecular probe. Even with an exposure time of 500 ms, the measured signal was extremely close to noise. The cells appeared to be quite uniformly stained by curcumin, including the nucleus. Also, lowering the concentration of curcumin-loaded nanocarriers or inhibition of endocytosis-mediated uptake using dynasore, sodium azide or treatment at 4 °C did not seem to have any effect on the fluorescent intensity (Appendix, figure A.1 and A.2).

Formalin-fixated cells and tissues are known to display some autofluorescence within the FITC range, as described in the introduction. To ensure that the weak observed signal was actually from curcumin and not caused by autofluorescence, cells were incubated with or without nanocarriers and fixed with formalin with or without DNA staining dye (HOECHST). A similar intensity in the curcumin channel (figure 3.7) was observed for cells incubated with or without nanocarriers (figure 3.7 a,c and b,d respectively), suggesting that the observed signal was mostly caused by autofluorescence. Interestingly, cells that were only exposed to nanocarriers (figure 3.8a and c) showed an even lower intensity then cells that were incubated with HOECHST.

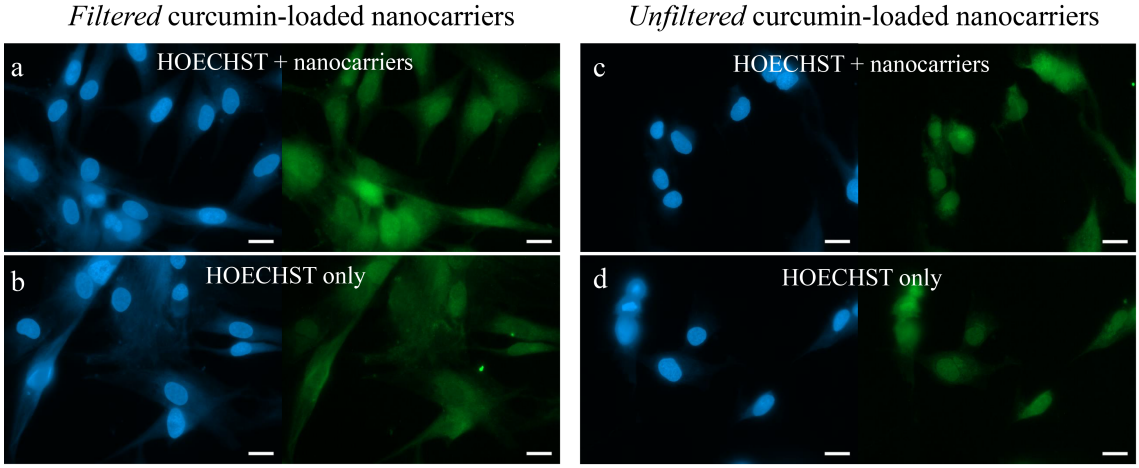

Figure 3.7: The fibroblasts were exposed to (a,c) nanocarriers or (b,d) DMEM for 5 min and all cells were fixated with 10% formalin, containing 1:1000 HOECHST dye. The HOECHST and curcumin channel are on the left and right, respectively. Exp. time = 150 ms HOECHST channel, 500 ms curcumin channel; Scale = 20 μm.

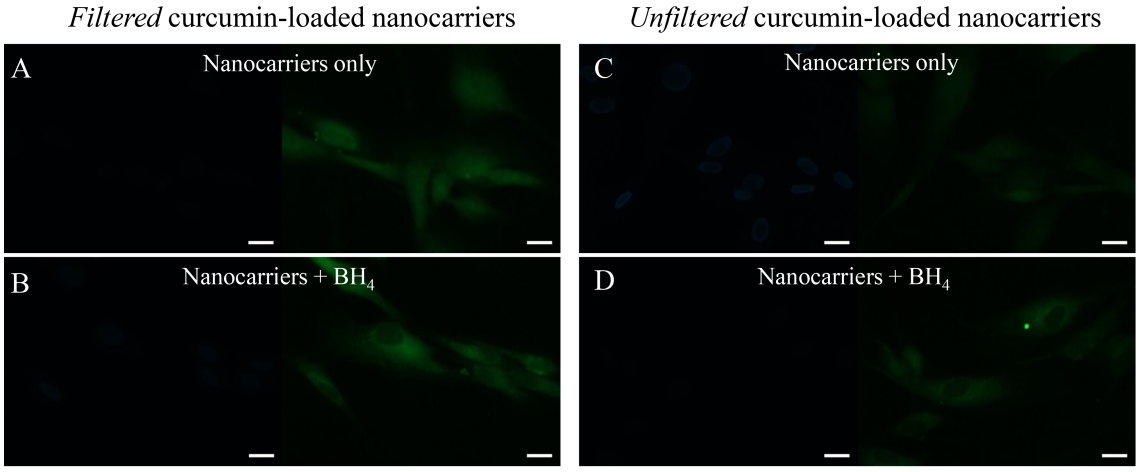

Figure 3.8: The fibroblasts were exposed to nanocarriers for 5 min and all cells were fixated with 10% formalin. the cells (b,d) were further treated with borohydrate. The HOECHST and curcumin channel are on the left and right, respectively. Exp. time = 150 ms HOECHST channel, 500 ms curcumin channel; Scale = 20 μm.

Some fixated cells were treated with borohydrate to quench the autofluorescence (figure

3.8b and d). This treatment removed most of the fluorescence inside the nucleus, but also caused photobleaching within seconds. Due to all the previously described complications, the fluorphore DiI was chosen as a new molecular probe and hydrophobic model drug. By using an actual fluorphore that emits at a higher wavelength, the influence of autofluorescence should be reduced and the signal quality improved.

3.2.2 Sonificated, DiI-loaded nanocarriers

The new sonificated, DiI loaded nanocarriers greatly improved the fluorescent signal, and the exposure time could be reduced from 500 ms to 50 ms. Furthermore, the nucleus of the cells did not show fluorescence. Therefore, fibroblasts were exposed to the loaded carriers with or without inhibitors. To ensure the cells had enough time to take up the nanocarriers, the incubation time was increased to 2 hours (figure 3.9).

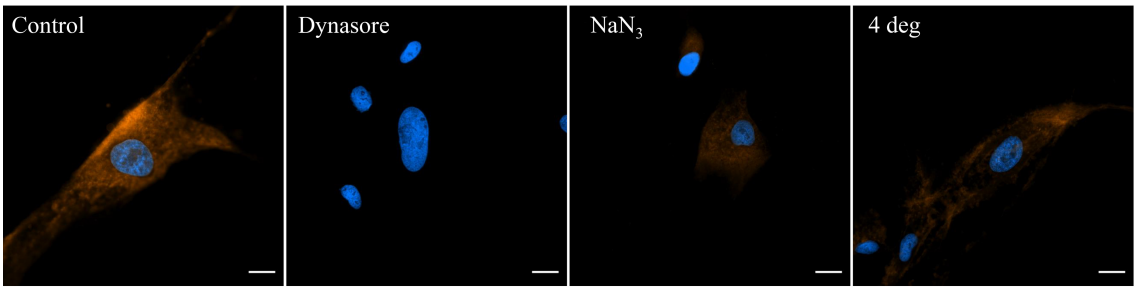

Figure 3.9: Merged HOECHST and DiI channels of fixated (10% formalin) fibroblasts exposed to 0.5 μg/mL DiI-loaded nanocarriers (2 h) and certain inhibitors/treatments (30 min pre-incubation, 25μg/mL dynasore, 0.1% NaN_3) . Exp. = 200 ms HOECHST channel, 50 ms DiI channel; Scale = 20 μm.

The same cloudy spread of fluorescent signal was observed in all conditions, except when exposed to the inhibitor dynasore. Treatment with sodium azide or uptake at 4 degrees did seem to reduce the fluorescent signal, possibly indicating reduced uptake. Again, lowering the concentration seemed to have no effect on the signal intensity (Appendix, figure A.3).

The absence of any DiI signal in the cells treated with dynasore can be explained. Dynasore seems to reduce the excitation and emission of DiI (Appendix, figure A.8). This phenomenon is not caused by dynasore absorbing around the excitation wavelength of DiI (Appendix, figure A.9). Possibly, dynasore enters the nanocarriers and interacts with DiI, reducing its fluorescent properties. Unfortunately, this makes the inhibitor useless to study the uptake of DiI-loaded nanocarriers.

The cloudy fluorescent cells were observed in all further experiments, until the cells were imaged before fixation (figure 3.10). Before fixation, distinct particles can be found inside the cell, which disappear after fixation. Different fixation techniques yielded the same result and the exact mechanism causing this effect has not been found. Therefore, all the proceeding cell experiments were imaged live.

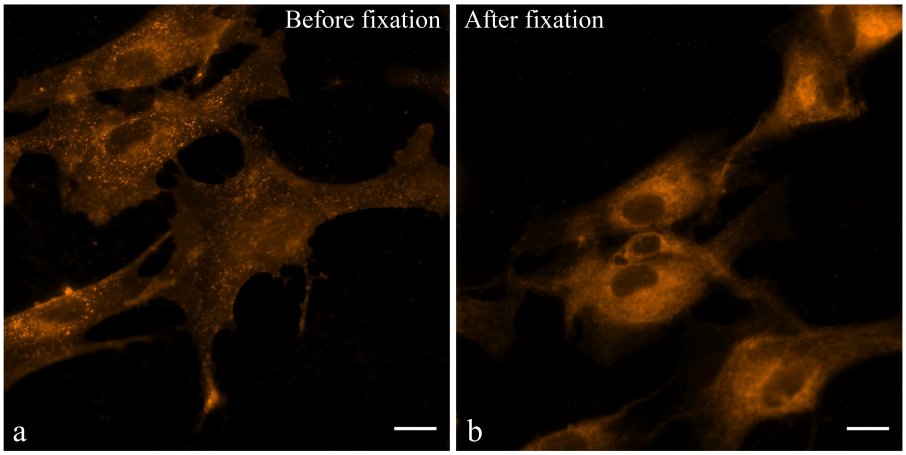

Figure 3.10: Fibroblasts exposed to 0.5 mg/mL DiI-loaded nanocarriers (2h) before (a) and after (b) fixation (10% formalin). Exp. = 100 ms (a) 50 ms (b) DiI channel; Scale = 20 μm.

To observe the progression of the nanocarrier uptake, an interval experiment was performed in which the cells were imaged at 10, 30, 60 and 120 min (figure 3.11). At 10 min (figure 3.11a) the nanocarriers are only found on the surface of the cells. Over time (30-60 min, figure 3.11b,c) the fluorescence signal seems to increase and more particles are embedded inside the membrane. After 2 hours (figure 3.11d) of incubation some particles can also be found inside the cell.

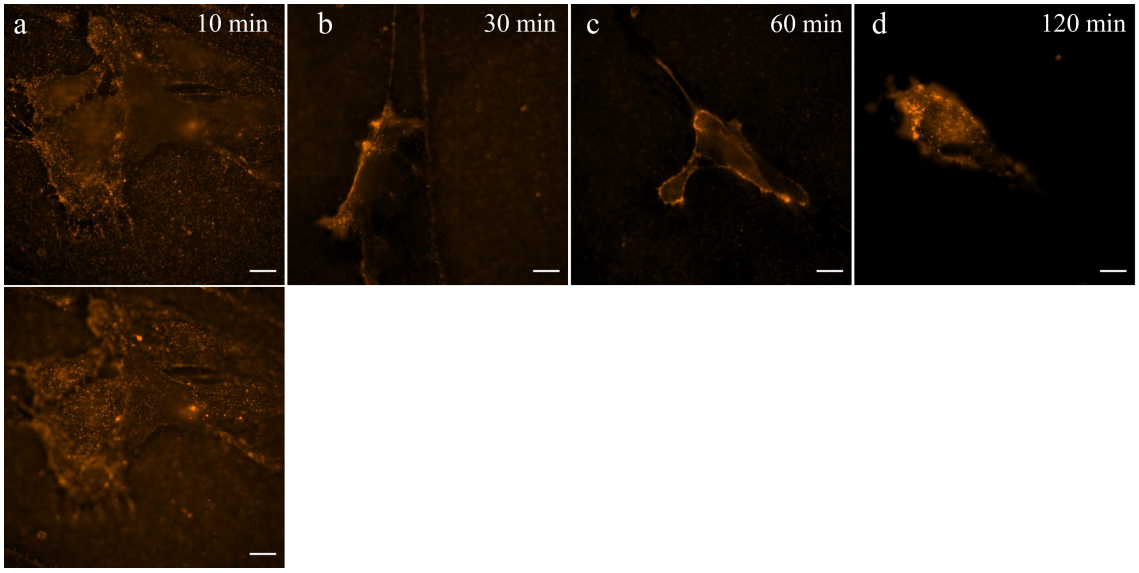

Figure 3.11: Live fibroblasts exposed to 0.5 mg/mL DiI-loaded nanocarriers. a) Shows two different focus planes of the same cell. Exp. = (a) 150 ms, (b) 100 ms (c) 50 ms, (d) 50 ms in DiI channel; Scale = 20 μm.

The previously reported sonificated, curcumin-loaded nanocarriers seemed to have the ability to enter the nucleus [3]. Therefore, sonificated, DiI-loaded nanocarriers were exposed to fibroblasts (2 h) and were imaged at different focal planes (z-stack, 40 slides, 0.28 μm apart). Figure 3.12 shows a deconvolution image at three different positions inside

the stack. Deconvolution is a post-processing technique that attempts to remove out of focus fluorescent signal from each plane. The images show that the nanocarriers follow the outside of the nucleus. At position z-15 some particles are just outside or on the nucleus membrane. z-18 shows the center slice of the nucleus which is completely void of particles, and z-23 shows the top of the nucleus, on which some carriers can be found, again. Non of the imaged cells showed any uptake of the nanocarriers inside the nucleus.

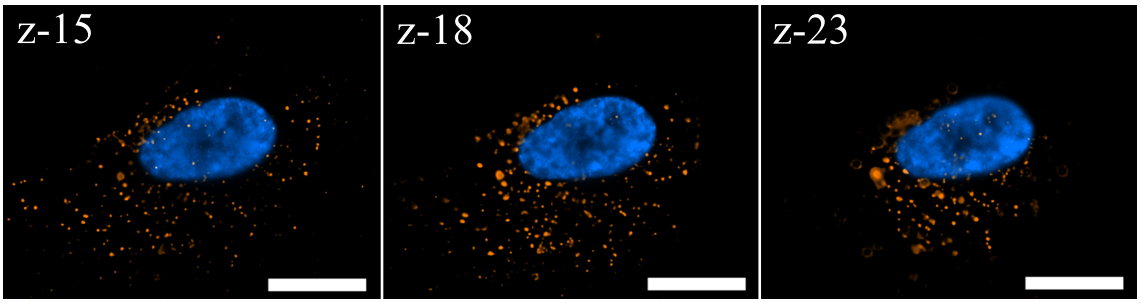

Figure 3.12: Deconvolution image of merged HOECHST and DiI channels of fibroblasts exposed to 0.5 μg/mL DiI-loaded nanocarriers (2 h) on three different positions inside a z-stack of 40, 0.28 μm apart. Exp. = 150 ms DiI channel, 150 ms HOECHST channel, Scale = 20 μm.

Finally, to further investigate the precise uptake mechanism, fibroblasts were again exposed to nanocarriers with different inhibitors or conditions (figure 3.13). This time, the cells were pre-incubated with the inhibitors 1 hour prior to exposure to the nanocarriers. The effect of dynasore on DiI has been explained above. Sodium azide treatment did not seem to alter the uptake. The cell that were exposed to the nanocarriers at 4 degrees Celcius do show a completely different pattern. The drug does not get taken up inside the cells, but stays on the outside, possibly slightly imbedded in the membrane. Indicating that the uptake is an energy dependent process. Figure A.4 gives a better look at the 4 degree treated cells.

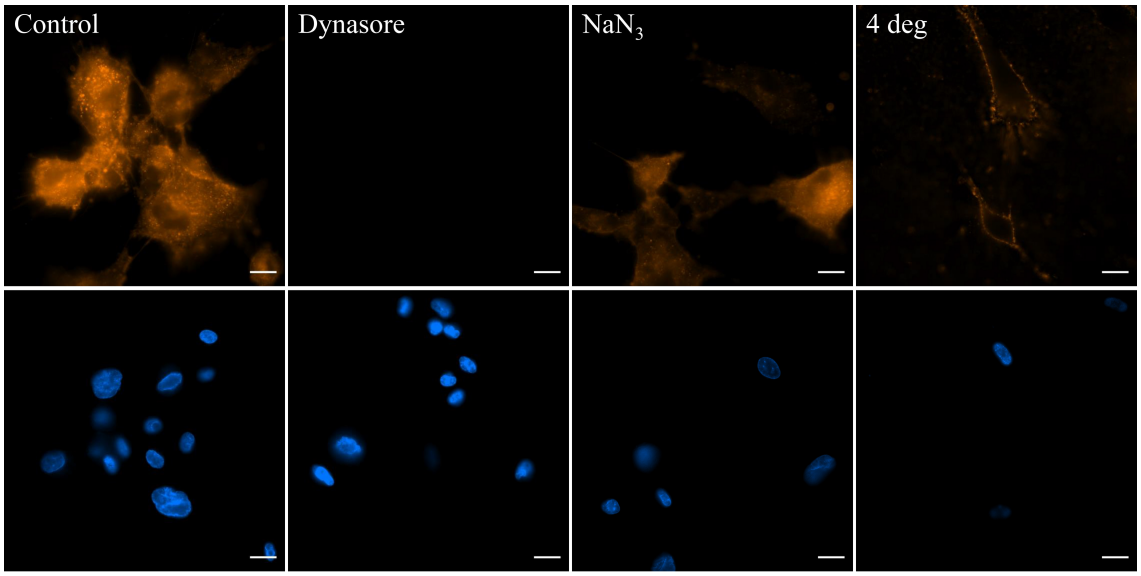

Figure 3.13: HOECHST (bottom) and DiI (top) channels of live fibroblasts exposed to 0.5 mg/mL DiI-loaded nanocarriers (2 h) and certain inhibitors/treatments (1 h pre-incubation, 25μg/mL dynasore, 0.1% NaN_3). Exp. = 150 ms HOECHST channel, 50 ms DiI channel; Scale = 20 μm.

3.2.3 Cosolvent evaporated, DiI-loaded nanocarriers

Since smaller (<100 nm) nanocarriers were believed to enter the nucleus [3], cosolvent evaporated, DiI-loaded nanocarriers were exposed to fibroblasts (2h) and imaged at different focal planes (z-stack, 35 slices, 0.28 μm apart). Figure 3.14 shows a deconvolution image at three different positions inside the stack. The results show that the nanocarriers follow the outside of the nucleus and do not appear inside of the nucleus (z-5 bottom of cell, below nucleus; z-15 center slice of nucleus; z-31 top part of the cell, above nucleus). This result was consistent in all the cells that were imaged.

To learn more about the actual trafficking of the nanocarriers after uptake, a LysoTracker was used. This dye stains all the acidic compartments inside the cell, therefore revealing the position of lysosomes and late endosomes. If the carriers undergo clathrin-dependent endocytosis or macropinocytosis, a majority of the drug is expected to be located in the lysosomes. Preliminary tests with only the LysoTracker showed good staining inside the cell (Appendix, figure A.5). A very weak signal in the DiI channel could also be observed, but would be easily overpowered by the real DiI signal.

Therefore, fibroblasts were incubated with the cosolvent evaporated nanocarriers for 2 hours and then stained with the LysoTracker. Figure 3.15 shows the separate and combined channels of the DiI-loaded nanocarriers and the LysoTracker. The amount of carriers found inside lysosomes differed greatly (figure 3.15a,b) between each cell, but at least some overlap was always found. This suggests that the drug ends up inside the lysosomes and possibly (partly) follow a classical endocytotic pathway.

The uptake mechanism was further studied by treating the cells with either sodium azide or

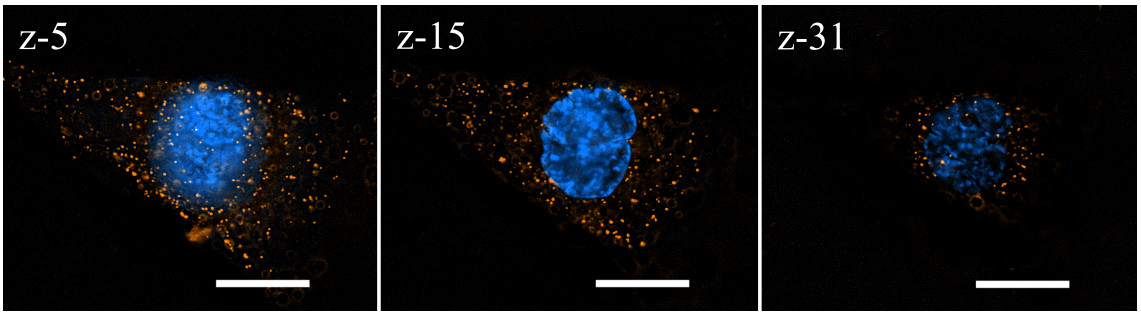

Figure 3.14: Deconvolution image of merged HOECHST and DiI channels of fibroblasts exposed to 0.2 mg/mL DiI-loaded nanocarriers (2 h). Three different positions inside a z-stack of 35, 0.28 μm apart. Exp. = 50 ms HOECHST channel, 200 ms DiI channel; Scale = 20 μm.

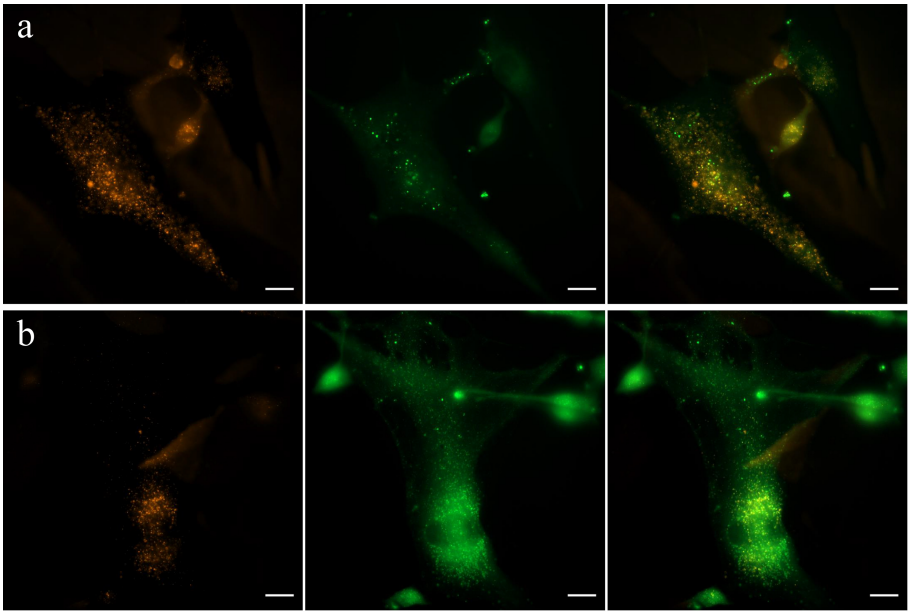

Figure 3.15: Image of DiI (left), LysoTracker (middle) and combined (right) channels of fibroblasts exposed to 0.2 mg/mL DiI-loaded nanocarriers (2 h). Exp. = 200 ms LysoTracker channel, 200 ms DiI channel; Scale = 20 μm.

incubating at 4 °C. First, the ideal sodium azide concentration was determined to be 0.1% (Appendix, figure A.6), since previously used concentrations lead to a lot of cell death. Treatment with the inhibitor dynasore was not included, since this inhibitor quenched the DiI fluorescence. The results can be found in figure 3.16 and show that treatment with sodium azide did not seem to alter the uptake of DiI, compared to the control. However, 4 °C treatment seemed to effectively reduce the uptake of DiI, indicating an energy-dependent uptake mechanism of the nanocarriers.

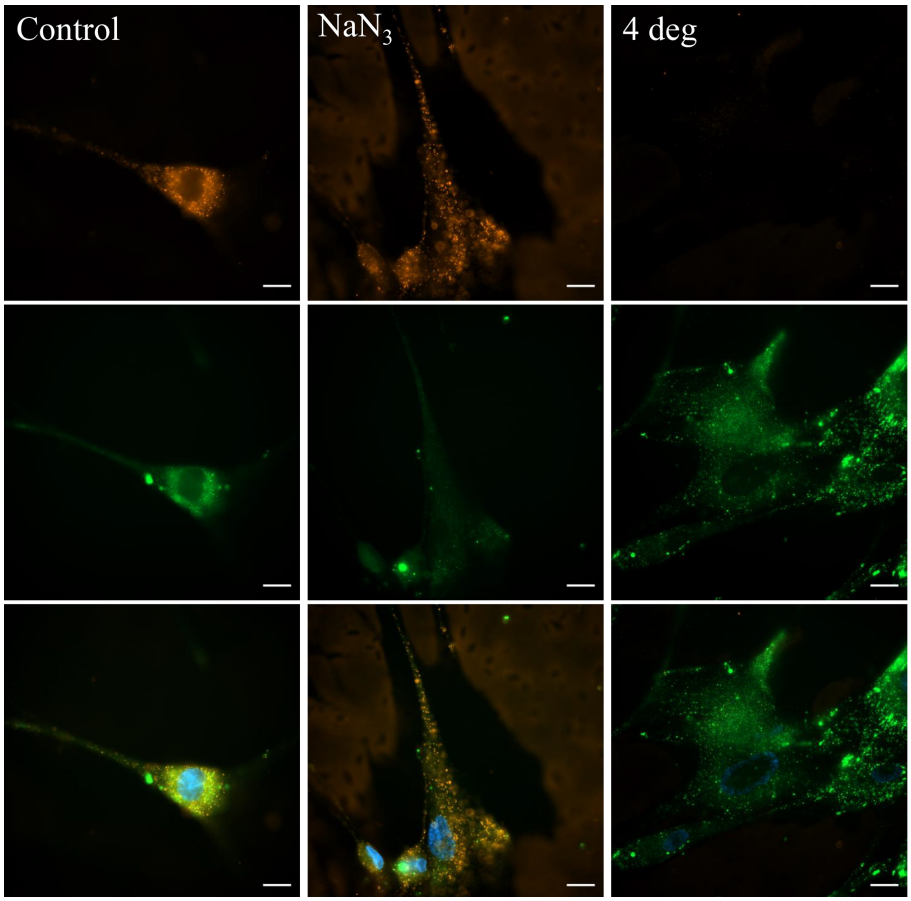

Figure 3.16: Image of DiI (top), LysoTracker (middle) and combined (bottom) channels of fibroblasts exposed to 0.2 mg/mL DiI-loaded nanocarriers (2 h) under different experimental conditions (1 h pre-incubation, 0.1% NaN_3). Exp. = 200 ms LysoTracker channel, 200 ms DiI channel, 200 ms HOECHST channel; Scale = 20 μm.

3.3 Comparison of sonificated and cosolvent evaporated nanocarriers

During this master thesis both sonificated and cosolvent evaporated nanocarriers were created. No major uptake differences in fibroblasts were observed, despite their differences in size. The sonificated nanocarriers did seem to stain the cell membrane more and did have a higher fluorescent intensity, possibly due to a higher drug loading of DiI. However, when the cells were depleted of energy (4 °C treatment) and exposed to the nanocarriers, a difference was observed. In both cases no drug was taken up inside the cells, but sonificated carriers seem to adhere or stick to the cell membrane even after the cells were washed. The cosolvent evaporated carriers did not show this behavior (figure 3.17)

To get some statistical data on this phenomenon, the exposed cells were also analyzed using flow cytometry. First the correct cell gates were selected (Appendix, figure A.17) and then a height histogram was produced for the DiI (PE) channel (figure 3.18). The figure clearly shows the difference in fluorescent intensity between sonificated and cosolvent evaporated

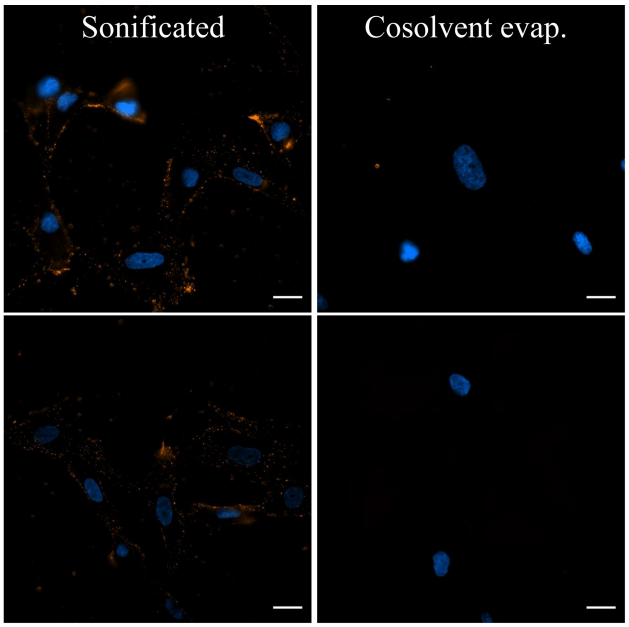

Figure 3.17: Image of merged HOECHST and DiI channels of fibroblasts exposed to 0.2 mg/mL sonifcated or cosolvent evaporated DiI-loaded nanocarriers (2 h). Exp. = 50 ms HOECHST channel, 200 ms DiI channel; Scale = 20 μm.

nanocarriers at 37 °C, most likely caused by a higher fluorphore loading in the sonificated carriers. Cells that were exposed to the nanocarriers at 4 °C do show a reduction in median fluorescent intensity (MFI) of 90% (sonificated) and 97% (cosolvent evaporated), compared to the 37 °C exposed cells. This clearly indicates that uptake of the nanocarriers is largely energy dependent. Interestingly, when compared to the control, 4 °C cells that were exposed to cosolvent evaporated nanocarriers do show an increased fluorescence. While not clearly observed in the fluorescent images, possibly some nanocarriers get absorbed onto the cell membrane.

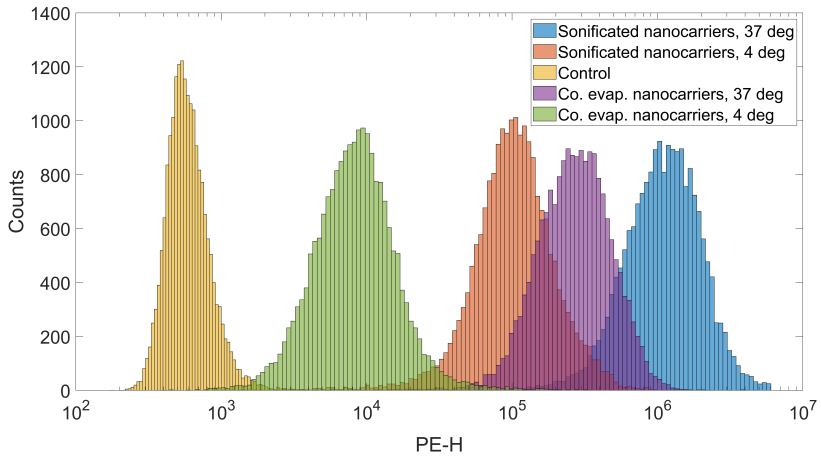

Figure 3.18: Fluorescent height-intensity histogram of fibroblasts exposed to sonificated and cosolvent evaporated nanocarriers under various conditions.

Discussion 4

4.1 Characteristics of PVP-OD nanocarriers

4.1.1 Negative-stain TEM

The size of the nanocarriers was determined by DLS and visualized using negative-stain TEM. Visualizing soft material with TEM can be rather tricky and cause artifacts that can be misinterpreted. Correctly stained samples show low contrast objects that have a darker halo contouring them. When objects appear darker than the surrounding the staining has failed [54]. Therefore, the obtained TEM images of the nanocarriers most likely do not give an accurate representation of the structures in solution, which is also reflected by the size differences observed between DLS and TEM. This unsuccessful staining could be caused by dehydration followed by stain absorbance [54]. It is recommended to optimize the negative staining for the future or use Cryo-TEM, which is a more informative technique and shows aggregates in a more native state [54, 55].

4.1.2 Dissolving PVP-OD

The PVP-OD block copolymers were designed to form polymeric micelles in aqueous solution, however the polymer has proven difficult to dissolve. When the polymer was directly dissolved in water, aggregates around 200 nm were formed. A PVP-OD micelle with fully stretched polymer chains is estimated to have a maximum length of 30 nm. Therefore, these aggregates cannot be polymeric micelles. Instead, an other (or multiple) type(s) of aggregates are formed. An attempt was made to load the core of these aggregates with a chelated europium complex, to be able to visualize the core using TEM. Unfortunately, the complex was to unstable to be efficiently loaded, resulting in crystal formation under TEM. Negative-stain TEM of the dissolved polymers showed round structures, but these results could be caused by improper staining (see above). Therefore, the structure(s) of the larger aggregates remains unknown.

The amphiphilic polymers dissolved in 80% ethanol had an average size around 30 nm, with a PDI of 0.313. While the obtained average size is more in line with the expected size of polymeric micelles, the size distribution is still rather broad. The distribution remains similar when the polymer is dissolved in THF or acetonitrile, while the average size shifts to 15 nm. Perhaps the polymer itself has a broad molecular weight distribution or different type of aggregates are also formed. The polymer was kindly given to us by Kulikov et al,

but information about molecular weight distribution was not provided [4]. In general, a narrower size distribution of polymeric micelles is favoured for drug delivery to avoid size-sieving in the bloodstream [56].
Hussein et al. gives an overview of polymeric micelles and their core/corona weight ratio [56]. Values range between 0.3 as minimum and 4.8 as a maximum ratio. The 12 kDa PVP-OD polymer has a core/corona ratio of 0.02 and is in that case very unconventional. Since the core/corona ratio of polymers is known to influence the size and uptake [57], it is recommended to also investigate PVP-OD polymers with a core/corona ratio that is more in line with established polymeric micelles.

4.1.3 DiI-loaded nanocarriers

The drug-loading of cosolvent evaporated nanocarriers was lower then that of sonificated nanocarriers. As explained in the theory, the solvent plays an important roll in the loading capacity of cosolvent evaporated nanocarriers [16]. If the drug aggregates out of solution before it can be captured by the nanocarriers, the loading capacity will be decreased. While acetonitrile and THF were better solvents for DiI and could dissolve PVP-OD, addition of water caused aggregation of the nanocarrier and could therefore not be used. However, other miscible solvents could still be tried such as DSMO or DMF. Unfortunately, the exact concentration of DiI-loaded nanocarriers has not been determined due to time constraints, but the method used by Mahmud et al. is recommended [57].
Another interesting characteristic that has not been measured is the drug release rate of the nanocarriers. In order to effectively transport the drug, the nanocarriers should be stable and prevent their cargo from releasing. Thus, knowing more about the release rate gives information about the stability of the carriers. Mahmud et al. makes use of multilamellar vesicles to measure drug release of DiI from PEO-b-PCL copolymers [57]. The same method could also be used for the DiI-loaded nanocarriers and is recommended for further research.

Both the sonificated and cosolvent evaporated, DiI-loaded nanocarriers were stable in DMEM medium for at least 3 hours, shown by DLS. Cosolvent evaporated, DiI-loaded nanocarriers started to form larger aggregates after three weeks at 4 °C. Ideally the nanocarriers could be lyophilized, to increase storage time and prevent premature drug release. While freeze-dried sonificated nanocarriers could be dehydrated, the cosolvent evaporated nanocarriers did not redissolve to their original size distribution (data not shown). Stabilization of the nanocarriers with lyoprotectants during freeze-drying might combat this problem [16].

Reproducing the same DiI-loaded nanocarriers distribution with cosolvent evaporation was difficult. Large particles (300-500 nm) were sometimes observed, that would pass over a 0.2 μm filter even if the sample was filtered multiple times. These particles were not observed in the start-mixture or water for cosolvent evaporation. It is therefore believed

that these aggregates are possibly smaller loosely attached aggregates that quickly reform after filtration. An approach to combat this problem has not yet been found.

4.2 Cell uptake experiments

Fibroblasts were exposed to both the sonificated and cosolvent evaporated nanocarriers, to study the uptake. Previously reported curcumin-loaded PVP-OD nanocarriers were believed to enter the nucleus of the cell depending on size [3]. The same nanocarrier production protocol (sonification method) was followed, but did not result in a similar size distribution. This might be caused by a difference in method to determine the size (NTA vs DLS) or because a different size PVP-OD polymer was used. Furthermore, the fluorescent signal of curcumin was to close to noise to obtain reliable fluorescent microscopy data. Therefore, DiI-loaded nanocarriers were prepared following the same sonification method, which greatly improved the fluorescent signal. In order to observe nanocarrier uptake the initial 10 minute incubation reported by Luss et al. had to be extended to 2 hours. The then observed uptake of DiI could only be found inside the cytosol.
The cosolvent evaporated, DiI-loaded, nanocarriers were made using a different technique, but have the $<$100 nm size that was thought to be responsible for uptake inside the nucleus. The drug (DiI) of these carriers was also only found to be taken up inside the cytosol. Luss et al. did not report the molecular weight of the PVP-OD polymer and different core/corona ratio's could alter the uptake mechanisms of nanocarriers [57]. However, the weakly observed curcumin signal in combination with the short incubation time, places some doubt in the conclusions drawn by Luss et al.

The measured signal during fluorescent microscopy is that of the model drug DiI and only gives information about the uptake of the drug. Other groups have reported interesting uptake mechanisms in which the drug, but not the nanocarrier itself, gets taken up [36, 58, 59]. Therefore, in order to confirm the uptake of the whole nanocarrier, fluorescent labeled nanocarriers should be created and colocalized with the drug. The cosolvent evaporated nanocarriers were compared with a LysoTracker, which stains all the acidic compartments of the cell. In all occasions, at least some overlap was found between the drug and the LysoTracker, indicating uptake of the drug via clathrin-mediated endocytosis and/or macropinocytosis. However, some care in colocalization is required, because some structures in close proximity could be seen as colocalized, because of poor resolution [60]. The uptake mechanisms of the DiI-loaded nanocarriers were further investigated by using specific endocytic inhibitors.

4.2.1 Endocytosis inhibitors

To investigate the endocytic mechanisms responsible for nanocarrier uptake in this thesis, different endocytosis inhibitors were used: 4 °C and sodium azide treatment to determine if the uptake was energy dependent and treatment with dynasore to inhibit all dynamin

dependent pathways.
4 °C treatment was a reliable and reproducible way to deplete the cells of energy, if at least 1 hour of pre-incubation time was used and all media were pre-cooled. This treatment seems to be the standard to assess energy dependent uptake [57, 61, 62].

Sodium azide treatment did not show similar results. Cells seemed unaffected and uptake of nanoparticles looked similar as the control. Possibly, the cells were not fully energy-depleted and could still perform endocytosis. The cells were pre-incubated with 0.1% sodium azide for 1 hr at 37 °C. Chen et al. used the same concentration and incubation time, but at 4 °C to deplete the cells of energy faster [36]. Shorter incubation times at a higher concentration (0.5%) have been reported [63], but lead to cell death in our set-up. In general, sodium azide is a hard treatment for cells and the exact concentration to not induce cell death, but efficient energy depletion, should be found for each cell line. Since sodium azide has such a cytotoxic effect and influences so many processes in cells, it might not be the most optimal inhibitor to study such an intricate process as endocytosis.

The results showed that dynasore reduced the fluorescent properties of DiI, making it an unsuitable inhibitor when combined with DiI-loaded nanocarriers. Initially, dynasore was believed to interact with DiI inside the nanocarrier, blocking its function, since dynasore did not seem to alter the size of the DiI-loaded nanocarriers (data not shown). However, other groups have used DiI as drug inside nanoparticles [64] or as LDL-tag [65] in combination with dynasore and did not observe this effect. Possibly, the observed reaction is nanocarrier specific and should be investigated further.

To gain a better understanding of the nanocarrier uptake pathway, new inhibitors should be tried. However, there are very few inhibitors that specifically inhibit one endocytic mechanism without side-effects, therefore it is recommended to use multiple inhibitors to verify the obtained results [60]. Some of the most common inhibitors can be found in the following review articles: [60, 63, 66].

4.3 Comparison of sonificated and cosolvent evaporated nanocarriers

Even though the sonificated and cosolvent evaporated nanocarriers had a different size distribution, not many differences between uptake in fibroblasts could be found. However, besides normal cellular uptake, sonificated nanocarriers did seem to stain the cell membrane more than cosolvent evaporated nanocarriers. This might be caused by a higher drug release rate of sonificated carriers, since free DiI can incorporate itself inside membranes. When the cells were depleted of energy by the 4 °C treatment, no uptake of the drug was observed. This was confirmed by flow cytometry, that showed that the median fluorescent intensity (MFI) was lowered by 90 or 97 percent for cosolvent evaporated and sonificated nanocarriers, respectively. This indicates that the uptake of the nanocarriers by fibroblasts

is largely energy-dependent. However, the sonificated nanocarriers were observed to be either slightly embedded inside the cell membrane or perhaps in clathrin or caveolae coated pits, while the cosolvent evaporated nanocarriers were not. This difference could be caused by the charge of the carriers and should be further investigated.

5 Conclusion

In this master thesis the characteristics of PVP-OD nanocarriers were investigated and the influence of their size on the uptake in fibroblasts (CRL 2429) examined. Therefore, nanocarriers with a diameter of 220 nm (0.2 PDI) were created via the sonification method. While an excellent model drug, curcumin had a too weak fluorescent signal to be measured with fluorescent microscopy. So, DiI-loaded nanocarriers were produced of the same size. Ethanol was found to be the best solvent for cosolvent evaporation and the stability of 12 kDa PVP-OD nanocarriers in water/ethanol could be improved, when water was adjusted to a pH 10. Nanocarriers with a diameter of 21 nm (0.244 PDI) were produced with the cosolvent evaporation method. These carriers were stable in DMEM medium for at least 3 hours and started to form larger aggregates after storage of three weeks at 4 °C.

Both nanocarriers were taken up by fibroblasts through an energy-dependent process. Inhibition led to a decrease of median fluorescent intensity (MFI) of 90 or 97 percent for sonificated and cosolvent evaporated nanocarriers, respectively. Fluorescent microscopy confirmed that no nanocarriers could be found inside the cytosol. However, sonificated nanocarriers would adhere to the cell membrane during 4 °C treatment, while cosolvent evaporated nanocarriers did not. Nanocarriers exposed to fibroblasts at 37 °C were only found inside the cytosol. No uptake inside the nucleus was observed. The drug of cosolvent evaporated nanocarriers could be colocalized with lysosomes (LysoTracker), possibly indicating uptake via macropinocytosis or clathrin-mediated endocytosis. However, further study with different endocytosis inhibitors is necessary to determine the exact uptake mechanism.

Bibliography

1. Li, Y., Yu, A., Li, L. & Zhai, G. The development of stimuli-responsive polymeric micelles for effective delivery of chemotherapeutic agents. *Journal of Drug Targeting* **26,** 753–765 (2018).
2. Bobo, D., Robinson, K. J., Islam, J., Thurecht, K. J. & Corrie, S. R. Nanoparticle-Based Medicines: A Review of FDA-Approved Materials and Clinical Trials to Date. *Pharmaceutical Research* **33,** 2373–2387 (2016).
3. Luss, A. L. *et al.* Nanosized carriers based on amphiphilic poly-N-vinyl-2-pyrrolidone for intranuclear drug delivery. *Nanomedicine* **13,** 703–715 (2018).
4. Kulikov, P. P., Kuskov, A. N., Goryachaya, A. V., Luss, A. N. & Shtil'man, M. I. Amphiphilic poly-n-vinyl-2-pyrrolidone: Synthesis, properties, nanoparticles. *Polymer Science, Series D* **10,** 263–268 (2017).
5. Kuskov, A. N. *et al.* Self-assembling nanoscaled drug delivery systems composed of amphiphilic poly-N-vinylpyrrolidones. *Journal of Non-Crystalline Solids* **353,** 3969–3975 (2007).
6. Rogero, S. O. *et al.* Biocompatibility Study of Polymeric Biomaterials. *Artificial Organs* **27,** 424–427 (2003).
7. Veeren, A., Bhaw-Luximon, A., Mukhopadhyay, D. & Jhurry, D. Mixed poly(vinyl pyrrolidone)-based drug-loaded nanomicelles shows enhanced efficacy against pancreatic cancer cell lines. *European Journal of Pharmaceutical Sciences* **102,** 250–260 (2017).
8. Ulbrich, K. *et al.* Targeted Drug Delivery with Polymers and Magnetic Nanoparticles: Covalent and Noncovalent Approaches, Release Control, and Clinical Studies. *Chemical Reviews* **116,** 5338–5431 (2016).
9. Cho, H., Lai, T. C., Tomoda, K. & Kwon, G. S. Polymeric Micelles for Multi-Drug Delivery in Cancer. *AAPS PharmSciTech* **16,** 10–20 (2014).
10. Torchilin, V. P. Structure and design of polymeric surfactant-based drug delivery systems. *Journal of Controlled Release* **73,** 137–172 (2001).
11. Gothwal, A., Khan, I. & Gupta, U. Polymeric Micelles: Recent Advancements in the Delivery of Anticancer Drugs. *Pharmaceutical Research* **33,** 18–39 (2016).
12. Stern, T. *et al.* Rigidity of polymer micelles affects interactions with tumor cells. *Journal of Controlled Release* **257,** 40–50 (2017).

13. Biswas, S., Kumari, P., Lakhani, P. M. & Ghosh, B. Recent advances in polymeric micelles for anti-cancer drug delivery. *European Journal of Pharmaceutical Sciences* **83,** 184–202 (2016).

14. Kim, S., Shi, Y., Kim, J. Y., Park, K. & Cheng, J.-X. Overcoming the barriers in micellar drug delivery: loading efficiency, in vivo stability, and micelle–cell interaction. *Expert Opinion on Drug Delivery* **7,** 49–62 (2010).

15. Jette, K. K., Law, D., Schmitt, E. a. & Kwon, G. S. Preparation and Drug Loading of Poly(Ethylene Glycol)-block-Poly(ϵ-Caprolactone) Micelles Through the Evaporation of a Cosolvent Azeotrope. *Science* **21,** 1184–1191 (2004).

16. Miller, T. *et al.* Drug loading of polymeric micelles. *Pharmaceutical Research* **30,** 584–595 (2013).

17. Canton, I. & Battaglia, G. Endocytosis at the nanoscale. *Chem. Soc. Rev.* **41,** 2718–2739 (2012).

18. Doherty, G. J. & McMahon, H. T. Mechanisms of Endocytosis. *Annual Review of Biochemistry* **78,** 857–902 (2009).

19. Sahay, G., Alakhova, D. Y. & Kabanov, A. V. Endocytosis of nanomedicines. *Journal of Controlled Release* **145,** 182–195 (2010).

20. Hillaireau, H. & Couvreur, P. Nanocarriers' entry into the cell: relevance to drug delivery. *Cellular and Molecular Life Sciences* **66,** 2873–2896 (2009).

21. Champion, J. A. & Mitragotri, S. Role of target geometry in phagocytosis. *Proceedings of the National Academy of Sciences* **103,** 4930–4934 (2006).

22. Champion, J. A., Katare, Y. K. & Mitragotri, S. Making polymeric micro- and nanoparticles of complex shapes. *Proceedings of the National Academy of Sciences* **104,** 11901–11904 (2007).

23. Conner, S. D. & Schmid, S. L. Regulated portals of entry into the cell. *Nature* **422,** 37–44 (2003).

24. Roth, T. F. & Porter, K. R. Yolk Protein Uptake in the Oocyte of the Mosquito Aedes Aegypti. L. *The Journal of Cell Biology* **20,** 313–332 (1964).

25. Ehrlich, M. *et al.* Endocytosis by random initiation and stabilization of clathrin-coated pits. *Cell* **118,** 591–605 (2004).

26. Stewart, M. P., Lorenz, A., Dahlman, J. & Sahay, G. Challenges in carrier-mediated intracellular delivery: Moving beyond endosomal barriers. *Wiley Interdisciplinary Reviews: Nanomedicine and Nanobiotechnology* **8,** 465–478 (2016).

27. Bareford, L. M. & Swaan, P. W. Endocytic mechanisms for targeted drug delivery. *Advanced Drug Delivery Reviews* **59,** 748–758 (2007).

28. Lai, S. K. *et al.* Privileged delivery of polymer nanoparticles to the perinuclear region of live cells via a non-clathrin, non-degradative pathway. *Biomaterials* **28,** 2876–2884 (2007).

29. Harush-Frenkel, O., Debotton, N., Benita, S. & Altschuler, Y. Targeting of nanoparticles to the clathrin-mediated endocytic pathway. *Biochemical and Biophysical Research Communications* **353,** 26–32 (2007).

30. Kirchhausen, T., Macia, E. & Pelish, H. E. Use of Dynasore, the small molecule inhibitor of dynamin, in the regulation of endocytosis. *Methods in enzymology* **438,** 77–93 (2008).

31. Preta, G., Cronin, J. G. & Sheldon, I. M. Dynasore - not just a dynamin inhibitor. *Cell Communication and Signaling* **13,** 24 (2015).

32. Jones, J. A., Starkey, J. R. & Kleinhofs, A. Toxicity and mutagenicity of sodium azide in mammalian cell cultures. *Mutation Research/Genetic Toxicology* **77,** 293–299 (1980).

33. Slameňová, D. & Gabelová, A. The effects of sodium azide on mammalian cells cultivated in vitro. *Mutation Research - Fundamental and Molecular Mechanisms of Mutagenesis* **71,** 253–261 (1980).

34. Bowler, M. W., Montgomery, M. G., Leslie, A. G. W. & Walker, J. E. How azide inhibits ATP hydrolysis by the F-ATPases. *Proceedings of the National Academy of Sciences* **103,** 8646 LP –8649 (2006).

35. Ishikawa, T., Zhu, B.-L. & Maeda, H. Effect of sodium azide on the metabolic activity of cultured fetal cells. *Toxicology and Industrial Health* **22,** 337–341 (2006).

36. Chen, H. *et al.* Release of hydrophobic molecules from polymer micelles into cell membranes revealed by Förster resonance energy transfer imaging. *Proceedings of the National Academy of Sciences* **105,** 6596–6601 (2008).

37. Wang, D. *et al.* Mechanisms of pH-Sensitivity and Cellular Internalization of PEOz-b-PLA Micelles with Varied Hydrophilic/Hydrophobic Ratios and Intracellular Trafficking Routes and Fate of the Copolymer. *ACS Applied Materials and Interfaces* **9,** 6916–6930 (2017).

38. Wang, J., Ma, W. & Tu, P. The mechanism of self-assembled mixed micelles in improving curcumin oral absorption: In vitro and in vivo. *Colloids and Surfaces B: Biointerfaces* **133,** 108–119 (2015).

39. Davis, A. S. *et al.* Characterizing and Diminishing Autofluorescence in Formalin-fixed Paraffin-embedded Human Respiratory Tissue. *Journal of Histochemistry and Cytochemistry* **62,** 405–423 (2014).

40. Monici, M. Cell and tissue autofluorescence research and diagnostic applications. *Biotechnology annual review* **11,** 227–256 (2005).

41. Kajimura, J., Ito, R., Manley, N. R. & Hale, L. P. Optimization of Single- and Dual-Color Immunofluorescence Protocols for Formalin-Fixed, Paraffin-Embedded Archival Tissues. *Journal of Histochemistry & Cytochemistry* **64,** 112–124 (2015).

42. Viegas, M. S., Martins, T. C., Seco, F. & do Carmo, A. An improved and cost-effective methodology for the reduction of autofluorescence in direct immunofluorescence studies on formalin-fixed paraffin-embedded tissues. eng. *European journal of histochemistry : EJH* **51,** 59–66 (2007).

43. Shilova, O. N., Shilov, E. S. & Deyev, S. M. The effect of trypan blue treatment on autofluorescence of fixed cells. *Cytometry Part A* **91,** 917–925 (2017).

44. Sun, Y. & Chakrabartty, A. Cost-effective elimination of lipofuscin fluorescence from formalin-fixed brain tissue by white phosphor light emitting diode array. *Biochemistry and Cell Biology* **94,** 545–550 (2016).

45. Clancy, B. & Cauller, L. J. Reduction of background autofluorescence in brain sections following immersion in sodium borohydride. *Journal of Neuroscience Methods* **83,** 97–102 (1998).

46. Instruments, M. *Inform White Paper: Dynamic Light Scattering, Common terms defined.* 2011.

47. MALVERN. Instruments. Technical note: Dynamic Light Scattering: An Introduction in 30 Minutes, 1–8.

48. Stetefeld, J., McKenna, S. A. & Patel, T. R. Dynamic light scattering: a practical guide and applications in biomedical sciences. *Biophysical Reviews* **8,** 409–427 (2016).

49. Brown, M. & Wittwer, C. Flow cytometry: principles and clinical applications in hematology. *Clinical chemistry* **46,** 1221–9 (2000).

50. Adan, A., Alizada, G., Kiraz, Y., Baran, Y. & Nalbant, A. Flow cytometry: basic principles and applications. *Critical reviews in biotechnology* **37,** 163–176 (2017).

51. Yallapu, M. M., Jaggi, M. & Chauhan, S. C. Curcumin nanoformulations: a future nanomedicine for cancer. *Drug discovery today* **17,** 71–80 (2012).

52. Rahimi, H. R., Nedaeinia, R., Sepehri Shamloo, A., Nikdoust, S. & Kazemi Oskuee, R. Novel delivery system for natural products: Nano-curcumin formulations. *Avicenna journal of phytomedicine* **6,** 383–98 (2016).

53. Bisht, S. *et al.* Polymeric nanoparticle-encapsulated curcumin ("nanocurcumin"): A novel strategy for human cancer therapy. *Journal of Nanobiotechnology* **5,** 1–18 (2007).

54. Franken, L. E., Boekema, E. J. & Stuart, M. C. Transmission Electron Microscopy as a Tool for the Characterization of Soft Materials: Application and Interpretation. *Advanced Science* **4,** 1–9 (2017).

55. Won, Y. Y., Brannan, A. K., Davis, H. T. & Bates, F. S. Cryogenic transmission electron microscopy (cryo-TEM) of micelles and vesicles formed in water by poly(ethylene oxide)-based block copolymers. *Journal of Physical Chemistry B* **106,** 3354–3364 (2002).

56. Hussein, Y. H. & Youssry, M. Polymeric micelles of biodegradable diblock copolymers: Enhanced encapsulation of hydrophobic drugs. *Materials* **11** (2018).

57. Mahmud, A. & Lavasanifar, A. The effect of block copolymer structure on the internalization of polymeric micelles by human breast cancer cells. *Colloids and Surfaces B: Biointerfaces* **45,** 82–89 (2005).

58. Till, U. *et al.* Drug release by direct jump from poly(ethylene-glycol-b-ϵ-caprolactone) nano-vector to cell membrane. *Molecules* **21** (2016).

59. Kerdous, R., Sureau, F., Bour, A. & Bonneau, S. Release kinetics of an amphiphilic photosensitizer by block-polymer nanoparticles. *International Journal of Pharmaceutics* **495,** 750–760 (2015).

60. Iversen, T. G., Skotland, T. & Sandvig, K. Endocytosis and intracellular transport of nanoparticles: Present knowledge and need for future studies. *Nano Today* **6,** 176–185 (2011).

61. Wang, J., Wang, L., Li, Y., Wang, X. & Tu, P. Apically targeted oral micelles exhibit highly efficient intestinal uptake and oral absorption. *International Journal of Nanomedicine* **13,** 7997–8012 (2018).

62. Allen, C., Yu, Y., Eisenberg, A. & Maysinger, D. Cellular internalization of PCL20-b-PEO44block copolymer micelles. *Biochimica et Biophysica Acta - Biomembranes* **1421,** 32–38 (1999).

63. Zaki, N. M. & Tirelli, N. Gateways for the intracellular access of nanocarriers: a review of receptor-mediated endocytosis mechanisms and of strategies in receptor targeting. *Expert Opinion on Drug Delivery* **7,** 895–913 (2010).

64. Le, M. Q. *et al.* Residence time and uptake of porous and cationic maltodextrin-based nanoparticles in the nasal mucosa: Comparison with anionic and cationic nanoparticles. *International Journal of Pharmaceutics* **550,** 316–324 (2018).

65. Rahaman, S. O., Zhou, G. & Silverstein, R. L. Vav protein guanine nucleotide exchange factor regulates CD36 protein-mediated macrophage foam cell formation via calcium and dynamin-dependent processes. *Journal of Biological Chemistry* **286,** 36011–36019 (2011).

66. Zhao, J. & Stenzel, M. H. Entry of nanoparticles into cells: The importance of nanoparticle properties. *Polymer Chemistry* **9,** 259–272 (2018).

Appendices A

A.1 Additional fluorescent microscopy images

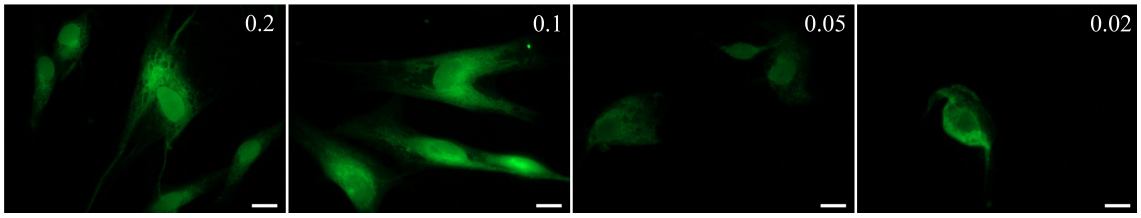

Figure A.1: Fluorescent image of fixated (10% formalin) fibroblasts exposed to different concentrations (mg/ml) of curcumin-loaded nanocarriers (5 min). Exp. = 500 ms curcumin channel; Scale = 20 μm

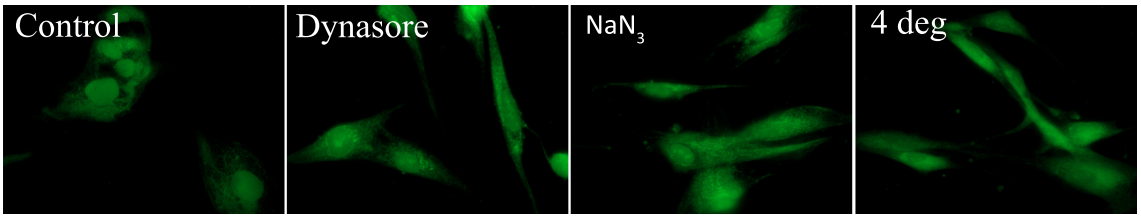

Figure A.2: Fluorescent image of fixated (10% formalin) fibroblasts exposed to 0.5 μg/mL curcumin-loaded nanocarriers (30 min) and certain inhibitors/treatments (pre-incubation 30 min, 25 μg/mL dynasore, 0.1% NaN_3) . Exp. = 500 ms curcumin channel; Scale = 20 μm

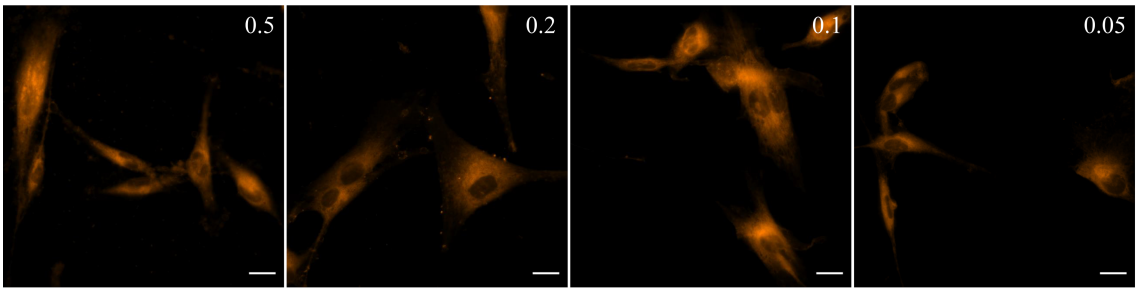

Figure A.3: Fluorescent image of fixated (10% formalin) fibroblasts exposed to different concentrations (mg/ml) of DiI-loaded nanocarriers (2 h). Exp. = 50 ms DiI channel; Scale = 20 μm

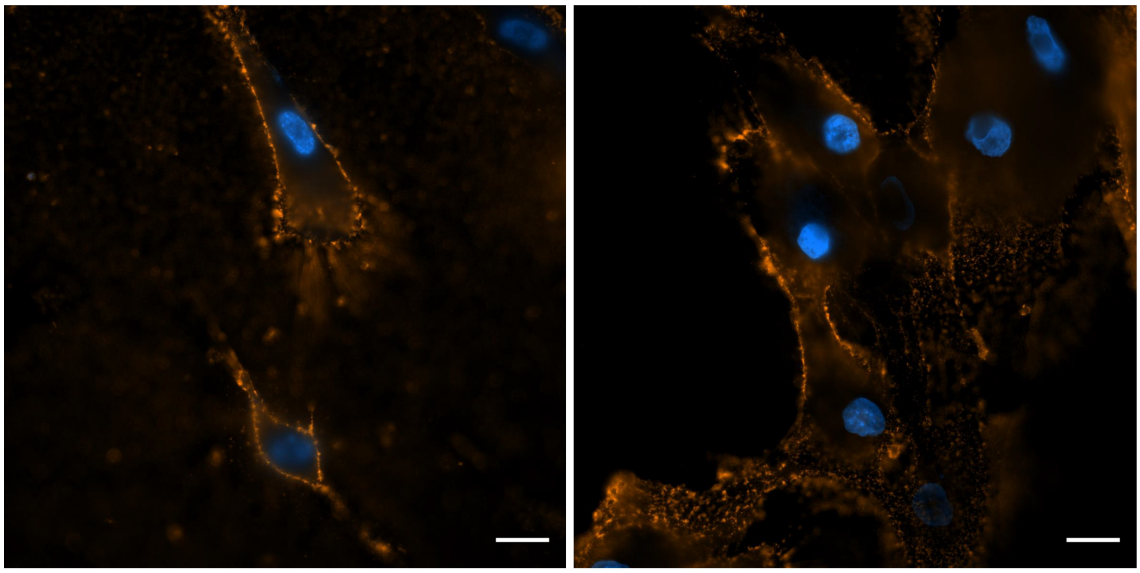

Figure A.4: Fluorescent images of combined HOECHST and DiI channels of fibroblasts exposed to 0.5 mg/mL DiI-loaded nanocarriers (2h) at 4 °C. Exp. = 50 ms DiI channel, 150 ms HOECHST channel; Scale = 20 μm.

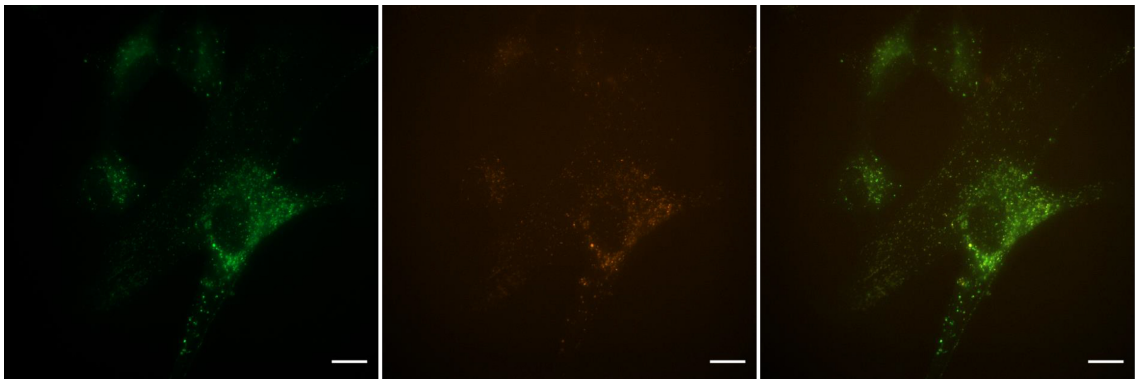

Figure A.5: Fluorescent image of fibroblasts incubated with 0.2 mg/mL DiI-loaded nanocarriers (2h) and stained with LysoTracker. left=LysoTracker, middle=DiI, right=combined channels. Exp. = 200 ms DiI channel, 200 ms LysoTracker; Scale = 20μm.

A.2 Sodium azide induced cell death

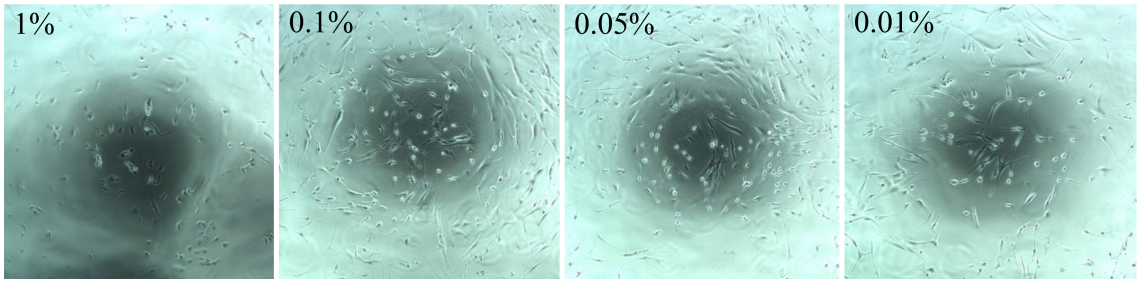

Figure A.6: microscopy images of fibroblasts treated with different sodium azide concentrations for 2.5 hours.

A.3 Original size distribution PVP-OD nanocarriers

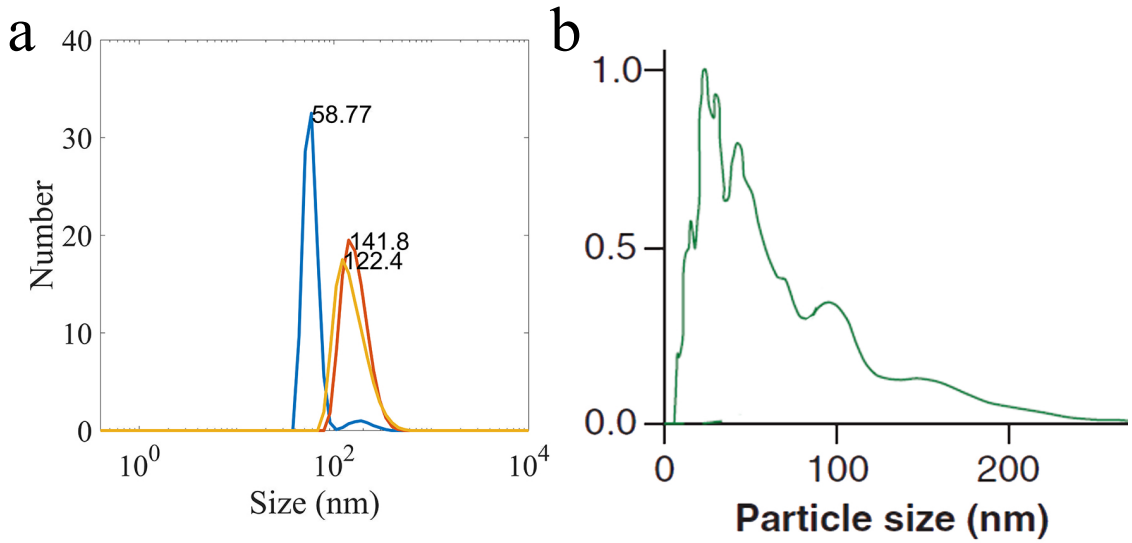

Figure A.7: Number distribution of (a) unfiltered, sonificated micelles by DLS and the (b) original distribution by NTA, taken from [3].

A.4 Cell culture protocols

The following pages include the basic protocols that were used during standard cell culturing procedures.

Basic growth medium

Materials:

- DMEM (Cat# BE12-604F, Lonza)
- FCS/FBS (Cat# 10270-106, Gibco)
- Penicillin/Streptomycin (10 KU/mL / 10 mg/mL, Cat# 15140-122, Invitrogen)
- Blue cap flask (Sterile)
- Filter top (22 µm)

Method:

All work takes place inside the flow bench! See volumes in scheme below.

1. Mix contents for the desired volume.
2. Screw the filter top onto the blue cap flask, and attach the filter to the vacuum system with the vacuum tube.
3. Pour the medium, FCS and Pen/Strep into the filter top, and turn the vacuum on.
4. When all of the medium has passed through the filter, turn vacuum off, and remove filter top. Close with the blue cap lid.
5. Mark the flask clearly with content, date and initials. Store the medium at 4° for no longer than 1 month.

	Conc. end				
DMEM F12		50 mL	100 mL	250 mL	500 mL
FCS	≈10 %	5 mL	10 mL	25 mL	50 mL
Pen/Strep	≈1 %	0,5 mL	1 mL	2,5 mL	5 mL

Comments:

Date and initials:

09-09-2015 RK

Defrosting cells

Materials:

- Basic growth medium
- T175 cell culture flask (Cat# 660175, Greiner)
- Pipet boy
- 25 mL stripette (Cat# 760180, Greiner)
- 100-1000 µL pipette
- 100-1250 µL pipette tips (cat# 613-1077, VWR)
- White plastic cup

Method:

All work takes place inside the flow bench!

1. Prepare the T175 cell culture flask with 30 mL basic growth medium. (Transfer from the blue cap flask with the stripette.) Place the T175 in the CO_2 incubator for 10-15 min. to prewarm the medium.
2. Put some lukewarm water in a white plastic cup, and bring it to the freezer storage room in the basement.
3. When the cells are located, place the cryo tube with cells in the lukewarm water and return to lab. (This step should be performed quickly, as the cryopreservation medium contains DMSO, which is toxic to the cells at temperatures above 0°C.)
4. Bring the T175 containing prewarmed basic growth medium to the flow bench. Dry the cryo tube congaing cells with a blue napkin, and clean it with 70 % EtOH from the spray bottle.
5. Transfer the cell suspension from the cryo tube to the T175 and “tilt” the flask to evenly distribute the cells.
6. Mark the culture flask with cell line, passage, date and initials before returning it to the CO_2 incubator.
7. After 24 h the medium should be changed to remove DMSO.

Comments:

Date and initials:

09-09-2015 RK

Changing medium

Materials:

- Basic growth medium
- Pipet boy
- Stripette
- White plastic cup

Method:

All work takes place inside the flow bench! See volumes in scheme below.

1. Prewarm the basic growth medium at RT for 20-30 min. to avoid chocking the cells by changing medium temperature from 37°C to 4°C.
2. When ready to begin, remove the medium from the cell culture flask by pouring it into the plastic cup.
3. Transfer the appropriate volume of medium from the blue cap flask with the stripette.
4. Return the cells to the CO_2 incubator.

Flask size	Medium	PBS	T/E
T175	30 mL	15 mL	3 mL
T75	15 mL	9 mL	1,5 mL
T25	5 mL	3 mL	1 mL

Comments:

Date and initials:

09-09-2015 RK

Sub culturing cells

Materials:

- Basic growth medium
- 1XPBS (Made from DPBS (10X) Cat# 14200-067, Gibco)
- Trypsin/EDTA (Cat# 15090-046, Invitrogen / Cat# 1.08418.0250, Bie & Berntsen)
- Cell culture flask (Greiner)
- Pipet boy
- Stripettes
- White plastic cup
- 15 mL centrifuge tube (Cat# 525-0150, VWR)

Method:

All work takes place inside the flow bench! See volumes in scheme below.

1. Prewarm the basic growth medium at RT for 20-30 min. to avoid chocking the cells by changing medium temperature from 37°C to 4°C.
2. When ready to begin, remove the medium from the cell culture flask by pouring it into the plastic cup.
3. Wash the cells by adding the appropriate volume of PBS, and gently tilting the flask. Remove PBS by pouring it into the white plastic cup. Repeat this X3 to remove proteins, as to much leftover protein will reduce the effect of the Trypsin/EDTA mix.
4. Add the appropriate volume of Trypsin/EDTA and distribute evenly in the flask by tilting it.
5. Incubate for 3-5 min. in the CO_2 incubator. Check progress by microscope, the cells should detach from the flask looking like this:

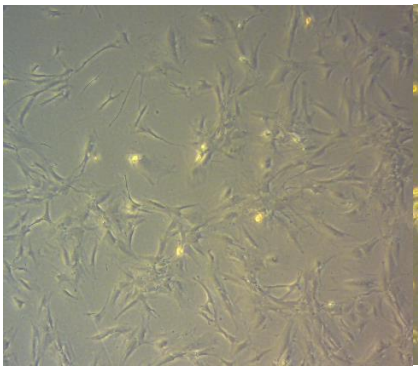

Figure 1 - Attached Cells

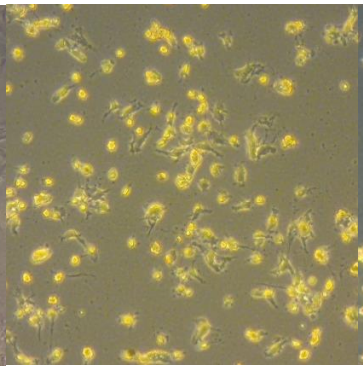

Figure 2 - Incomplete detachment

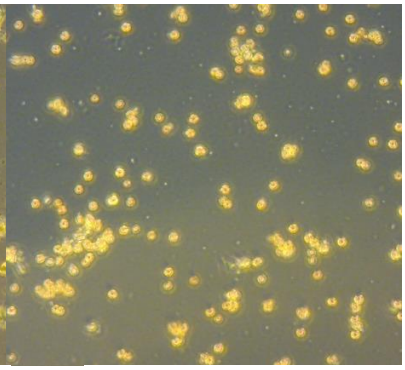

Figure 3 - Detached cells

6. When the cells are completely detached, add basic growth medium equivalent to X3 the volume of Trypsin/EDTA, to inactivate the Trypsin/EDTA and avoid the cells from being destroyed. Mix thoroughly.
7. Transfer the cell suspension to a 15 mL centrifuge, and spin the cells down at 300 xG for 5 min. at RT.
8. Discard supernatant by pouring it into the white plastic cup. Resuspend cells thoroughly in basic 5 mL growth medium.

9. To further cultivate the cells, transfer 1/5 to a new culture flask containing the appropriate volume of basic growth medium. Mark the flask clearly with cell line, passage, date and initials, before placing it in the CO_2 incubator.

Flask size	Medium	PBS	T/E
T175	30 mL	15 mL	3 mL
T75	15 mL	9 mL	1,5 mL
T25	5 mL	3 mL	1 mL

Comments:

Date and initials:
09-09-2015 RK

Counting cells

Materials:

- Basic growth medium
- 1XPBS (Made from DPBS (10X) Cat# 14200-067, Gibco)
- Trypsin/EDTA (Cat# 15090-046, Invitrogen / Cat# 1.08418.0250, Bie & Berntsen)
- Pipet boy
- Stripettes
- 1-10 µL pipette
- 0,1-10 µL pipette tips (Cat# 613-1082, VWR)
- White plastic cup
- 15 mL centrifuge tube (Cat# 525-0150, VWR)
- 650 µL micro centrifuge tubes (Cat# 211-0024, VWR)
- 0,4 % Trypan Blue (Cat# 93595, Sigma-Aldrich)
- Counting chamber

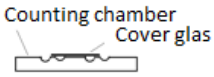

Method:

All work takes place inside the flow bench!

1. Prewarm the basic growth medium at RT for 20-30 min. to avoid chocking the cells by changing medium temperature from 37°C to 4°C.
2. When ready to begin, remove the medium from the cell culture flask by pouring it into the plastic cup.
3. Detach cells by following step 3 to 8 in the protocol for sub culturing cells.
4. Clean the counting chamber and cover glass with 70 % EtOH and a blue napkin, before assembling it by breathing on the chamber, and sliding/pressing the cover glass in place.
5. Thoroughly mix the cell suspension, and transfer 10 µL to a 650 µL micro centrifuge tube.
6. Add 10 µL 0,4 % trypan blue to the tube and mix thoroughly.
7. Apply 10 µL of the mix to the counting chamber by placing the tip on the counting chamber right by the edge of the cover glass. Capillary effect will pull the mix in place under the cover glass.
8. Place the counting chamber under an inverted phase microscope using the x10 magnification. It will look like this:

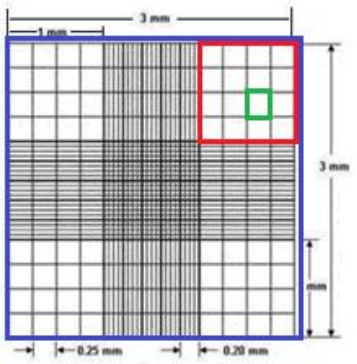

9. Count all four of the squares marked with red on the figure, in order to calculate a cell concentration (cells/mL) or a total number of cells. Make sure only to count live cells. The dead cells will have been stained by the trypan blue.
10. To calculate cell concentration use

$$\frac{\text{Number of cells countet}}{\text{4 squares}} (\cdot \text{ Dilution factor}) \cdot 10^4 = \text{X cells/mL}$$

The dilution factor will usually be 2 due to the 1:2 addition of trypan blue.

To calculate the total number of cells use

$$\text{X cells/mL} \cdot \text{ Y mL cell suspension} = \text{Z cells}$$

11. Proceed with seeding cells out for set up or further culturing.

Comments:

Date and initials:
09-09-2015 RK

Cryopreserving cells

Materials:

- Basic growth medium
- DMSO (Cat# D2650, Sigma-Aldrich)
- FCS/FBS (Cat# 10270-106, Gibco)
- Pipet boy
- Stripettes
- Pipettes (100-1250 µL / 20-200 µL)
- Pipette tips (Cat# 613-1077 / 613-1079, VWR)
- White plastic cup
- Cryo tubes (Cat# WC/696603, TH Geyer)
- Box of ice

Method:

All work takes place inside the flow bench!

5. Prewarm the basic growth medium at RT for 20-30 min. to avoid chocking the cells by changing medium temperature from 37°C to 4°C.
6. When ready to begin, remove the medium from the cell culture flask by pouring it into the plastic cup.
7. Calculate cell concentration by following the protocol for Counting cells.
8. Spin cells down at 300 xG for 5 min. at RT. Discard supernatant by pouring it into the white plastic cup.
9. Resuspend cells to a concentration of $2 \cdot 10^6$ cells/mL in basic growth medium. (This is in order to get a final concentration of approx. $1{,}5 \cdot 10^6$ cells/mL.)
10. Distribute the cell suspension into cryo tubes with 695 µL in each. Add 230 µL FCS to each tube.
11. Add 75 µL DMSO to one tube at a time. Mix thoroughly and place on ice immediately(!), before moving on to next tube.
12. Remember to mark each tube clearly with cell line, passage, date and initials before placing them in a small polystyrene box at -80°C. Move the cells to -140°C after 24 h.

Comments:

Date and initials:

09-09-2015 RK

Waste handling

Plastic utensils

All used plastic utensils are thrown in the waste bag by the door. When the bag is full, tie it up with green string, and label it with a yellow *"Genteknologisk lab. område klasse 1"* sticker. Bring it to the autoclave room (2.301) on the 2nd floor.

Cell and medium waste

When the bottle marked *"Cell waste"* is full almost, make sure the lid is properly closed, write the date on the back of it, and bring it to the autoclave room (2.301) on the 2nd floor for heat inactivation of antibiotics and proper termination of the cells.

Glass ware and reusable utensils

With cell contact

Clean glass and utensils properly in water. Make sure to dispose the rinsing water in the cell waste bottle! Leave a little bit of water in the bottom of glass ware, place reusable utensils in a cup containing some water. Glass ware and reusable utensils should be placed in the red plastic box.

Without cell contact

Clean glass and utensils properly in water. Place the glass wear and reusable utensils in the large grey container by the sink.

Comments:

Date and initials:

09-09-2015 RK

A.5 Macro's for statistical analysis TEM

A.5.1 Convert image to binary image

The following script/macro was used to convert the obtained TEM images to a binary image and was run using ImageJ (1.52n) macro plugin. The rolling parameter should be adjusted depending on the images.

```
// Only works when images are in a folder with no subfolders!!
// select right folder

path    = getDirectory("Choose a Directory");
list    = getFileList(path);
length  = list.length;

// create new folder to save processed images to

File.makeDirectory(path + "Processed/");

// Loop to substract background + binary

for (i=0; i<length; i++) {

    n=i+1;
    open(path+list[i]);
    img = File.nameWithoutExtension();
    selectWindow(img+".BMP");

run("Subtract Background...", "rolling=50 light");
run("Make Binary");
run("Erode");
run("Open");

// Save in created folder with same image name as original

saveAs ("Tiff", path + "Processed/" + img);
run("Close All");
}
```

A.5.2 Convert binary image to area of particle

The following script/macro was used to convert the binary images to particle area and was run using ImageJ (1.52n) macro plugin. The size parameter (size=25-Infinity) should be adjusted depending on the images.

```
// Only works when images are in a folder with no subfolders!!
// select right folder

path    = getDirectory("Choose a Directory");
list    = getFileList(path);
length  = list.length;

// create new folder to save processed images to

File.makeDirectory(path + "Size/");

// Loop to substract background + binary

for (i=0; i<length; i++) {
    n=i+1;
    open(path+list[i]);
    img = File.nameWithoutExtension();
    selectWindow(img+".tif");

run("Analyze Particles...", "size=25-Infinity show=Outlines display exclude include record");
selectWindow("Drawing of "+img+".tif");

// Save in created folder with same image name as original

saveAs("tiff", path + "Size/" + img);
}

// Save in created folder as .txt file

saveAs("results", path + "Size/Results.txt");
run("Close All")
```

A.6 Influence dynasore on DiI

The nanocarriers and dynasore were dissolved in DMEM to a concentration of 0.5 mg/mL and 25 μg/mL, respectively.

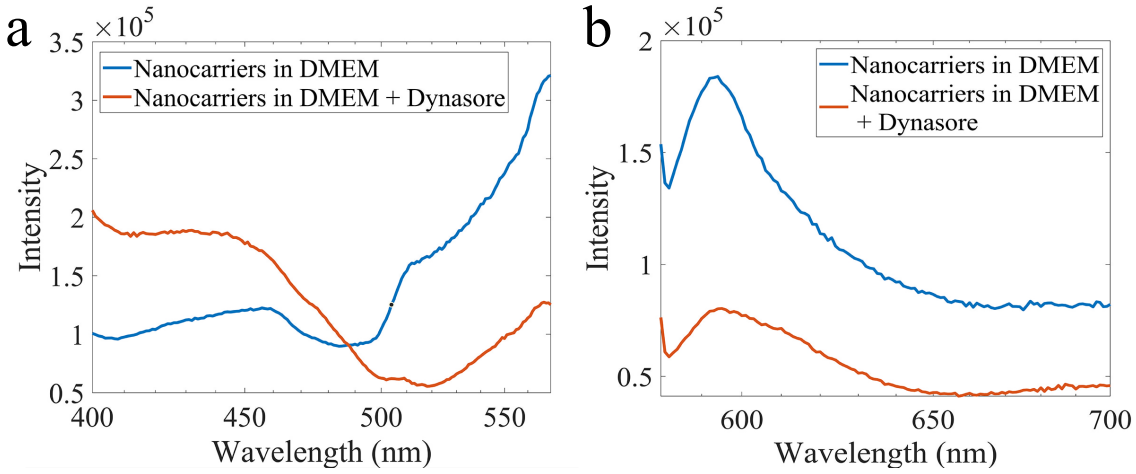

Figure A.8: Measured (a) excitation and (b) emission spectra of sonificated, DiI-loaded nanocarriers in DMEM with or without dynasore.

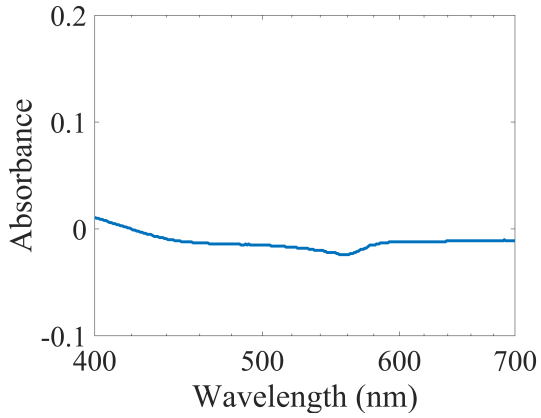

Figure A.9: Absorbance spectra of dynasore in DMEM

A.7 Optimizing solvent for PVP-OD

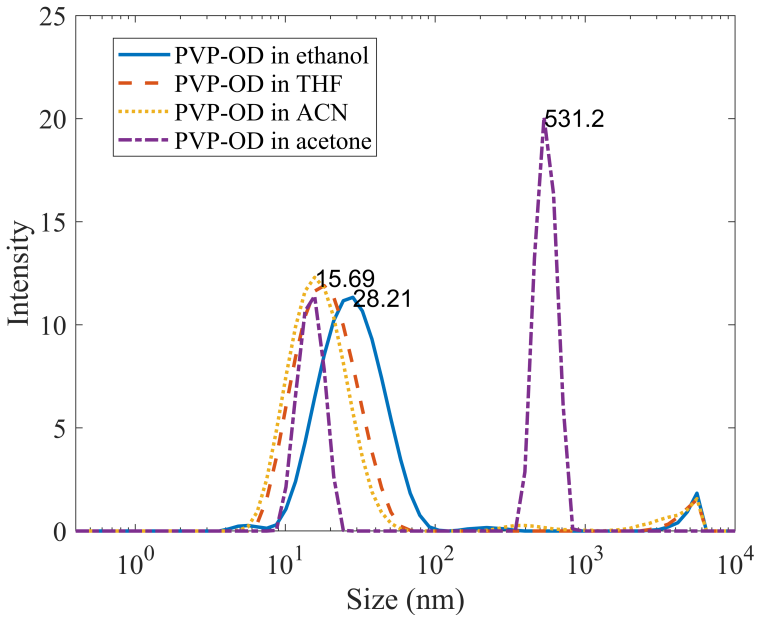

Figure A.10: Average (triplo) intensity distribution of 12kDa PVP-OD dissolved in various solvents

A.8 Additional TEM images

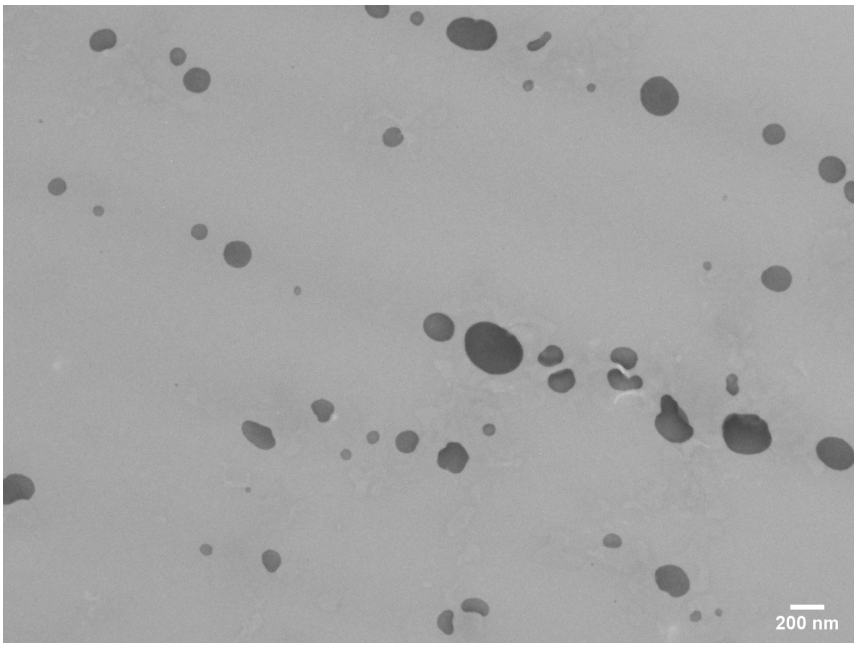

Figure A.11: Shape of unfiltered nanocarriers was not always round. Stained with 0.5% PTA.

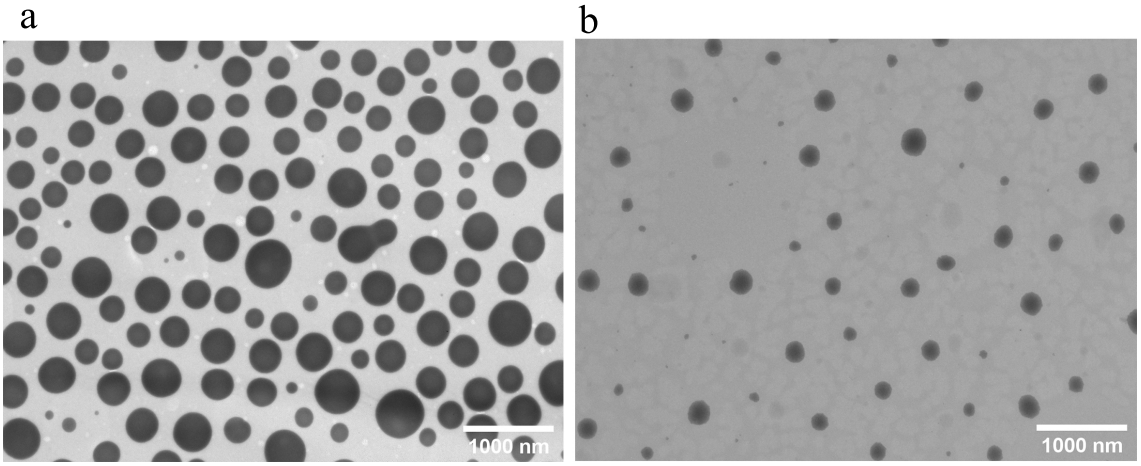

Figure A.12: a) Empty nanocarriers in 80% ethanol are not stable on TEM, but (b) pH adjusted seems to retain more smaller particles. Stained with 0.5% PTA.

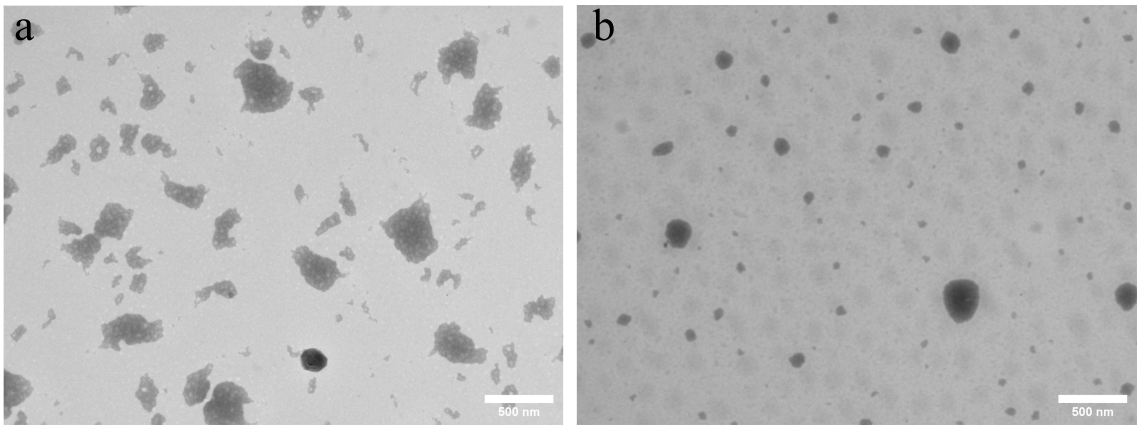

Figure A.13: TEM image of (a) neutral (b) and pH-10 adjusted cosolvent evaporated nanocarriers. Stained with 0.5% PTA.

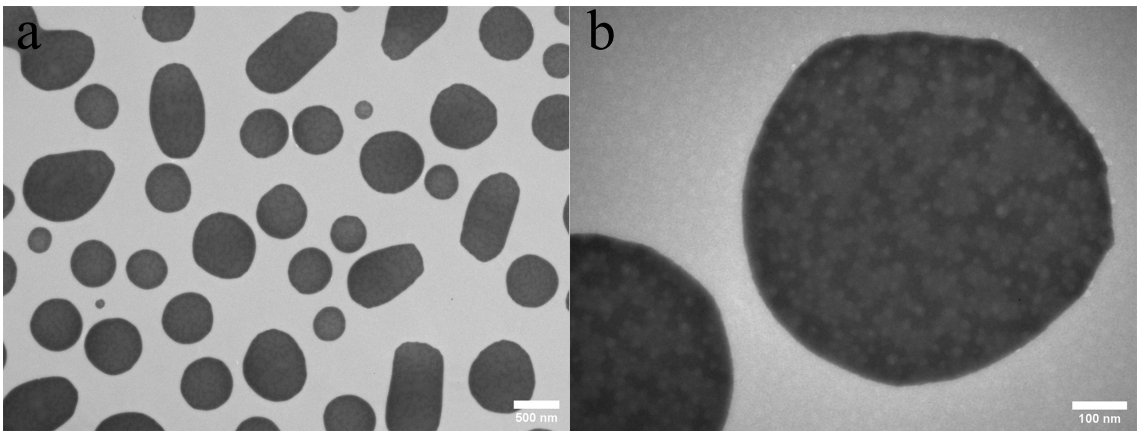

Figure A.14: TEM images of three week old, cosolvent evaporated, DiI-loaded nanocarriers. Stained with 0.5% PTA.

A.9 Europium complex

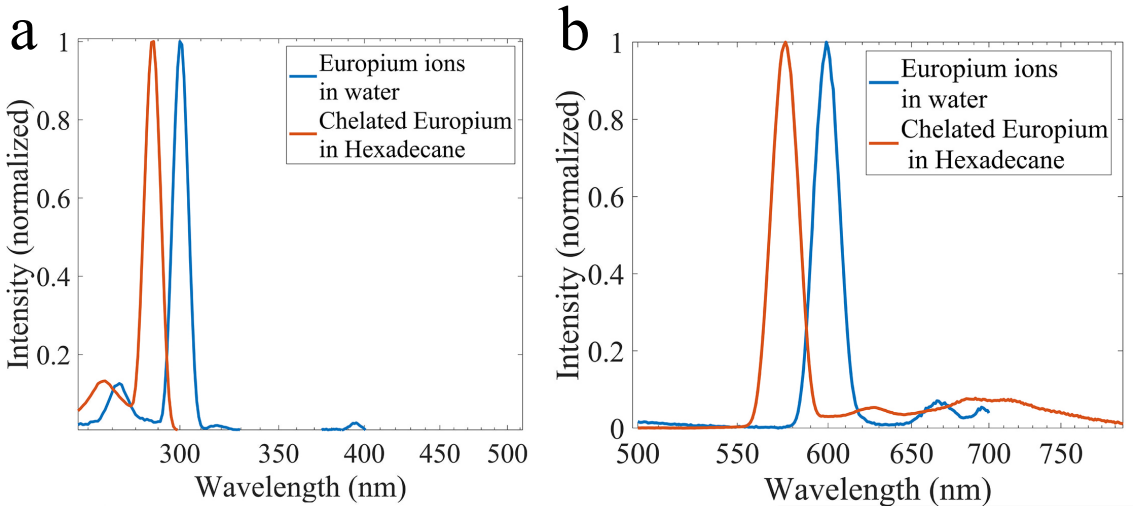

Figure A.15: Normalized (a) excitation and (b) emission spectrum of free and chelated Europium.

A.10 Large aggregates cosolvent evaporation method

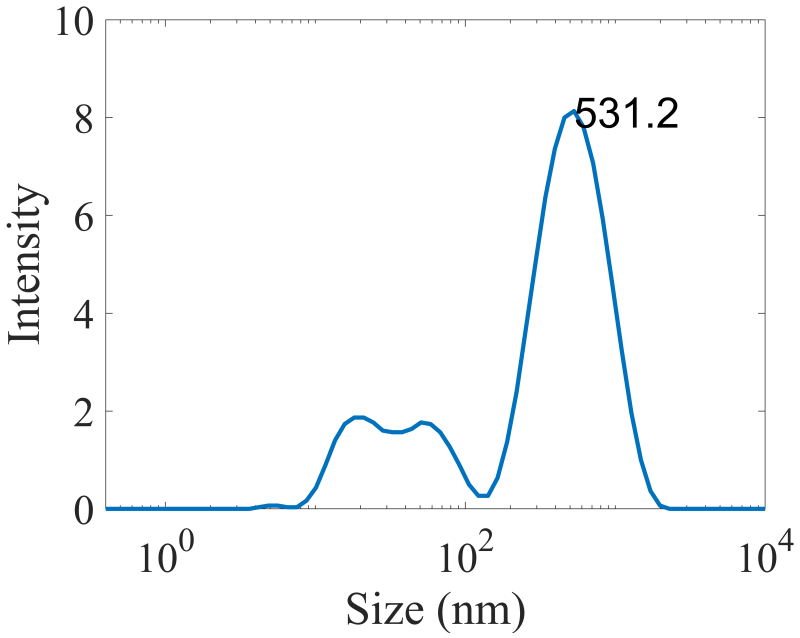

Figure A.16: Average (triplo) intensity distribution of cosolvent evaporated, DiI-loaded nanocarriers.

A.11 Gate flowcytometry

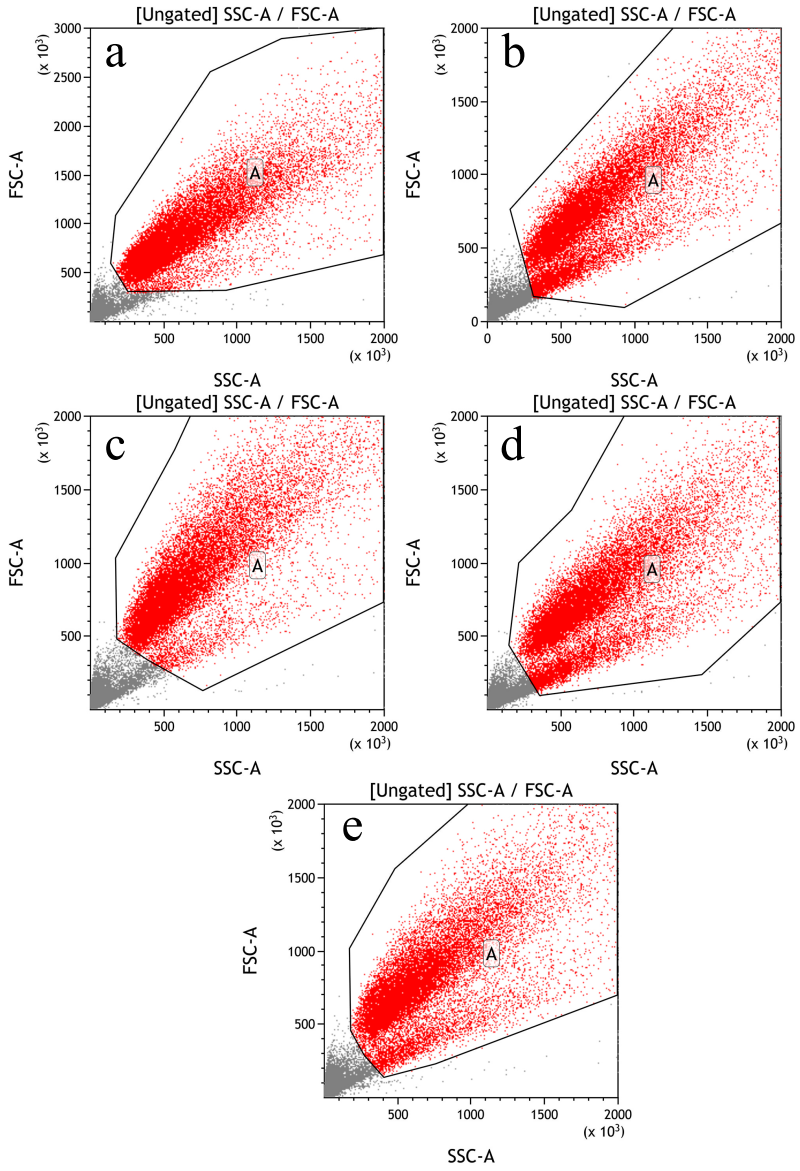

Figure A.17: Selected gates for flow cytometry analysis: fibroblasts incubated with 0.2 mg/mL of (a) sonificated nanocarriers (b) at 4 degrees. (c) cosolvent evaporated nanocarriers (d) at 4 degrees and (e) untreated fibroblasts (control).